Biochimica et Biophysica Acta 1787 (2009) 657–671

Contents lists available at ScienceDirect

Biochimica et Biophysica Acta

journal homepage: www.elsevier.com/locate/bbabio

Review

From protons to OXPHOS supercomplexes and Alzheimer's disease: Structure–dynamics–function relationships of energy-transducing membranes

H. Seelert [a,*], D.N. Dani [a], S. Dante [b], T. Hauß [a,b], F. Krause [a], E. Schäfer [a], M. Frenzel [a], A. Poetsch [a,1], S. Rexroth [a,1], H.J. Schwaßmann [a], T. Suhai [a], J. Vonck [c], N.A. Dencher [a,b,*]

[a] Physical Biochemistry, Department of Chemistry, Technische Universität Darmstadt, Petersenstrasse 22, D-64287 Darmstadt, Germany
[b] Helmholtz-Zentrum Berlin für Materialien und Energie, Lise-Meitner-Campus, Glienicker Strasse 100, D-14109 Berlin, Germany
[c] Max Planck Institute of Biophysics, Max-von-Laue-Strasse 3, D-60438 Frankfurt am Main, Germany

ARTICLE INFO

Article history:
Received 16 December 2008
Received in revised form 20 February 2009
Accepted 20 February 2009
Available online 10 March 2009

Keywords:
ATP synthase
Bacteriorhodopsin
Respiratory chain
Oxidative phosphorylation
β-amyloid peptide

ABSTRACT

By the elucidation of high-resolution structures the view of the bioenergetic processes has become more precise. But in the face of these fundamental advances, many problems are still unresolved. We have examined a variety of aspects of energy-transducing membranes from large protein complexes down to the level of protons and functional relevant picosecond protein dynamics. Based on the central role of the ATP synthase for supplying the biological fuel ATP, one main emphasis was put on this protein complex from both chloroplast and mitochondria. In particular the stoichiometry of protons required for the synthesis of one ATP molecule and the supramolecular organisation of ATP synthases were examined. Since formation of supercomplexes also concerns other complexes of the respiratory chain, our work was directed to unravel this kind of organisation, e.g. of the OXPHOS supercomplex $I_1III_2IV_1$, in terms of structure and function. Not only the large protein complexes or supercomplexes work as key players for biological energy conversion, but also small components as quinones which facilitate the transfer of electrons and protons. Therefore, their location in the membrane profile was determined by neutron diffraction. Physico-chemical features of the path of protons from the generators of the electrochemical gradient to the ATP synthase, as well as of their interaction with the membrane surface, could be elucidated by time-resolved absorption spectroscopy in combination with optical pH indicators. Diseases such as Alzheimer's dementia (AD) are triggered by perturbation of membranes and bioenergetics as demonstrated by our neutron scattering studies.

1. Introduction

The discovery of ATP in the year 1929 [1,2] paved the way to unravel the biochemical pathways that lead to the production of this ubiquitous energy currency in all organisms. In the subsequent years, all main components of respiration in mitochondria and of photosynthesis in plants were identified. But the essential link from electron transport to the final stage of forming the terminal high-energy phosphoanhydride bond in ATP remained nebulous for a long time. Mitchell's chemi-osmotic theory of energy coupling via an electrochemical proton gradient solved this issue in an artful way [3]. Another fundamental concept, discussed in the same context, implied the significance of conformational changes. This approach of Boyer explained the function of the ATP synthase by the binding-change mechanism [4–6]. Recently, the view of the bioenergetic processes has become more precise by the elucidation of many high-resolution structures that replaced early schematic drawings, as exemplified in Fig. 1 for the respiratory chain.

For major components of the mitochondrial respiratory chain, at least partial structures or structures from prokaryotic homologues are available. One of the biggest challenges remains the NADH:ubiquinone oxidoreductase (complex I), composed of more than 40 different subunits [7–11]. As shown schematically in Fig. 1, the shape and size of complex I is resolved by single particle analysis [12–15]. Additional data arise from crystal structures of subcomplexes, e.g. the hydrophilic domain [16]. However, merging structural data from different organisms is still demanding [17]. The subsequent complexes of the standard respiratory chain are resolved in more detail. For the

Abbreviations: AFM, atomic force microscopy; AD, Alzheimer's disease; Aβ, amyloid-β peptide; BN, blue-native; BR, bacteriorhodopsin; CBBG-250, Coomassie Brilliant Blue G-250; CF_1F_O, chloroplast ATP synthase; (C)F_O, membrane integral part of the (chloroplast) ATP synthase; CHAPS, 3-[3(cholamidopropyl)dimethylammonio]-1-propanesulfonate; CL, cardiolipin; CN, colourless native/clear native; CoQ_{10}, ubiquinone; DIGE, difference gel electrophoresis; F_1, hydrophilic part of the ATP synthase; OXPHOS, oxidative phosphorylation; PM, purple membrane; QENS, quasielastic neutron scattering; ROS, reactive oxygen species; ULV, unilamellar vesicles

* Corresponding authors. Tel.: +49 6151 16 5193; fax: +49 6151 164171.
E-mail addresses: seelert@hrzpub.tu-darmstadt.de (H. Seelert), nad@hrzpub.tu-darmstadt.de (N.A. Dencher).
[1] Present address: Plant Biochemistry, Ruhr-University Bochum, Universitätsstrasse 150, D-44801 Bochum, Germany.

0005-2728/$ – see front matter © 2009 Elsevier B.V. All rights reserved.
doi:10.1016/j.bbabio.2009.02.028

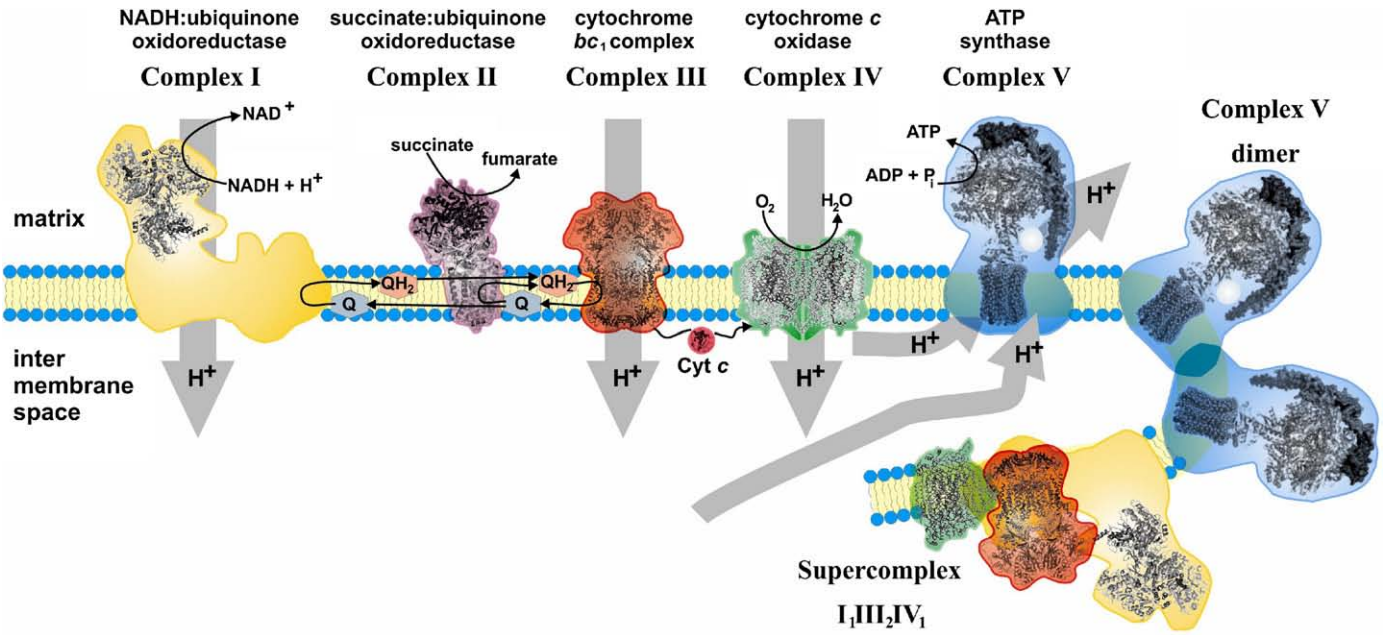

Fig. 1. Schematic representation of the OXPHOS complexes in the inner mitochondrial membrane. Electrons are transferred from NADH or succinate to the terminal acceptor molecular oxygen. Key components of this process are large transmembrane protein complexes (complexes I–IV) and the smaller mobile electron carriers ubiquinone and cytochrome *c*. Complexes I, III and IV generate thereby an electrochemical proton gradient across the membrane (symbolised as gray arrows). The ATP synthase utilises this gradient to produce the energy currency ATP. The representation of complex I bases on the shape from a single particle analysis of the *Yarrowia lipolytica* complex [12] intuitively combined with the X-ray structure of the soluble domain from *Thermus thermophilus* [16]. The illustration of complex II includes the crystal structures from the porcine heart enzyme [19]. For the complexes III [20] and IV [26] the homo-dimeric forms from bovine heart mitochondria are shown. In case of the ATP synthase, X-ray data from the F_1 portion together with the c-ring [29] and from the peripheral stalk [30] were fitted in the contour from single particle analysis of the complete bovine heart mitochondrial complex V [31].

succinate:ubiquinone oxidoreductase, as direct link to the citric acid cycle, a prokaryotic homologue (the fumarate-reductase [18]) but also complex II from porcine heart [19] have been characterised by X-ray crystallography. Upon solving the structure of the ubiquinol:cytochrome *c* oxidoreductase (complex III or cytochrome bc_1), a homo-dimeric form was revealed for bovine heart [20,21] and other mitochondria [22,23]. Likewise, the cytochrome *c* oxidase emerged as a dimer in crystals from prokaryotic [24,25] or mammalian [26] complex IV. Similar to the approach stated for complex I, pieces of a puzzle have to be combined for the representation of the ATP synthase. Therefore, X-ray structures of subcomplexes [27–30] were integrated into low-resolution single particle maps of complete F_1F_O-ATP synthases [31,32].

But in face of these fundamental advances, many problems are still unresolved and even new questions arise since novel or improved methods allow focusing on specific items. We have examined a variety of aspects of energy-transducing membranes from large protein complexes and supercomplexes down to the level of functional relevant picosecond protein dynamics and vectorial proton transfer applying diverse methods to reveal particulars of a sophisticated ensemble. Based on the central role of the ATP synthase for supplying the biological fuel ATP, one main emphasis was put on this protein complex. In particular the stoichiometry of protons required for the synthesis of one ATP molecule (Fig. 1; see Section 2.6) and the supramolecular organisation of ATP synthases also in respect to its modulation by the metabolism (see Section 2.7) were examined. Formation of supercomplexes not only concerns the ATP synthase but also other complexes of the respiratory chain (Fig. 1). Therefore, another main focus of our work was directed to unravel this kind of organisation, in terms of function (see Section 2.8) and structure (see Section 2.9), e.g. of the OXPHOS supercomplex $I_1III_2IV_1$. Moreover, the influence and consequences of supramolecular assemblies in context with ageing and mitochondrial diseases were studied (see Section 2.10). Perturbation of membranes, especially of mitochondrial membranes, may cause diseases such as Alzheimer's dementia (AD) (see Section 2.11). Not only the large protein complexes or supercomplexes work as key players for biological energy conversion, but also small mobile components as quinones which facilitate the transfer of electrons and protons (Fig. 1; see Section 2.3). Even as the chemi-osmotic theory explains important principals of biological energy conversion, the path of protons from the generators of the gradient to the ATP synthase is still highly debated (Fig. 1; see Section 2.1).

2. Deciphering structure–dynamics–function relationships

2.1. Electrochemical coupling of proton-transporting membrane proteins: water molecules as vehicles for proton translocation and lubricant for membrane dynamics

In mitochondria and chloroplasts, protein complexes generating electrochemical proton gradients and the proton ATP synthases powered by the gradient are spatially separated. Since the postulation of the chemi-osmotic hypothesis in 1961 [3], there is the ongoing debate to date on the pathway and kinetics of proton transfer between source and sink. In the previous three decades, studies employing the photon-driven proton pump bacteriorhodopsin (BR) had a great impact to answer many questions concerning proton translocation across membranes and along membrane surfaces, as summarised in Ref. [33]. For example, the pioneering experiments by Racker and Stoeckenius in 1974 demonstrating light-generated ATP formation in reconstituted BR/ATP synthase liposomes [34] unambiguously proved that Mitchell's chemosmotic hypothesis is fact (and paved the avenue to his award of the Nobel Prize). BR, the prototype of an integral membrane protein, especially of the family of seven membrane-spanning α-helical proteins, is one of the best characterised active ion-translocating proteins. Its vectorial transport mechanism is unravelled nearly at atomic level. An advantage of BR is the possibility to monitor the kinetics and stoichiometry of proton pumping by flash absorption spectroscopy in combination with optical pH indicators [35–37]. In this way, it was shown that only one proton per cycling BR

is released during the first part of the photocycle [36]. By employing optical pH indicators bound selectively to both membrane surfaces, vectorial proton transfer steps across BR and along the membranes surface were kinetically and spatially resolved and the possibility of efficient long distance proton transfer between source and sink demonstrated [37,38]. Upon light excitation, concomitant with the rise of the key photocycle intermediate M ($\tau_{mean}=83$ μs at 20 °C), a proton is pumped from the interior of BR to the extracellular surface ($\tau=90$ μs). The pumped proton dwells for about 1 ms at the membrane surface before it is released into the aqueous bulk phase ($\tau=1100$ μs). Under physiological conditions, the cytoplasmic surface of BR has to pick up protons from the well-buffered, slightly alkaline matrix. Attraction of protons from the medium and funnelling these protons into the orifice of the cytoplasmic proton channel are enhanced by a cluster of exposed carboxylates, acting as proton-collecting antenna [39–41]. The late phases of the photocycle are characterised by subsecond equilibration reactions where the protein regains protons from the bulk phase. This slow protonation reaction is attributed to a slow proton hole migration inside BR to the cytoplasmic surface. The proton transfer from D96 to the deprotonated Schiff base generates the proton hole and when it reaches the D38 domain, a proton from the bulk rapidly fills it [42]. Selective replacement of charged residues in the inter-helical loops modulates the rate of proton hole propagation, as well as the ionic strength of the solution.

All protons vectorially pumped are diffusing laterally along the membrane surface for long distances (several thousand Å) before equilibrating into the aqueous bulk phase. Protons move more slowly at the membrane–water interphase (diffusion coefficient $D_{app}=1\cdot10^{-6}$ cm^2/s at 20 °C; about 240 nm in 150 μs [38]) than in the aqueous bulk phase ($D=9.3\cdot10^{-5}$ cm^2/s). However, due to the surprisingly slow surface to bulk transfer rate (about 1 ms) protons can laterally diffuse macroscopic distances along the membrane surface. Since the translational diffusion of water molecules is 4.4 times faster [33,43] than the measured H^+ transfer rate along the surface, diffusing water molecules can act as vehicles. H^+ transfer along a membrane surface via water molecules could significantly contribute to, or even dominate, chemi-osmotic energy coupling.

At high hydration, the lipid head group region of membrane surfaces is more hydrated than the protein [44–46]. The hydration water of membrane surfaces has peculiar properties. For example, freezing of water occurs several degrees below the freezing point of bulk water (supercooled membrane water) and the first surface layer does not transform into the crystalline state, even below 240 K ("nonfreezing water") [33,43]. Water molecules at the membrane surface show anisotropic (only parallel to the membrane plane) two-dimensional long-range translational diffusion ($D_s=4.4\cdot10^{-6}$ cm^2/s), about five times slower than in bulk water [43]. Translational diffusion in the direction perpendicular to the membrane surface is not observable during the time window of picoseconds. This extraordinary behaviour of the surface hydration water in combination with the high buffer capacity of surface exposed amino acids and lipid head groups [47] might be the reason for the observation of efficient long distance lateral proton diffusion along the membrane surface before equilibration into the aqueous bulk phase.

Bacteriorhodopsin has contributed a lot to our understanding of bioenergetics, especially of molecular mechanisms. It has elucidated reaction pathways of proton transfer and the functional importance of water in membranes. Presently, BR is the best understood protein in respect to the hydration dependence of function and dynamics, as well as to the properties of the hydration water. From all the data gathered, the importance of water molecules for the function, structure, and dynamics of membranes is established, as well as for other photoactive proteins too [48]. Water molecules are key elements of the proton transport mechanism by providing a proton pathway and proton acceptor/donor groups. The proton-conducting pathway of BR contains at least 9 internal water molecules [44,46] that are thought to be key players in the proton translocation mechanism. By a multinuclear (^{1}H, ^{2}H, ^{17}O) magnetic relaxation dispersion study the rate of exchange of these internal water molecules with bulk water has been determined. At least 5 water molecules in BR have residence times in the range 0.1–0.5 μs at 277 K [49]. Most or all of the deeply buried water molecules in BR exchange on a time scale that is short compared to the rate-limiting step in the photocycle. In addition, water molecules "lubricate" the picosecond molecular motions and the light-triggered micro- to millisecond tertiary structural changes of the protein [33,43]. Furthermore, the hydration water at the membrane surface with its peculiar properties participates in long-range proton transfer, mediating bioenergetic coupling between the proton sources and sinks, such as the H^+-ATP synthase.

As the details of the molecular mechanisms of membrane proteins come into focus, our ignorance of the role of lipids stands in stark contrast. The role of specific lipid structures, such as cardiolipin (CL), in biological membranes has been elusive. CL is unique among phospholipids with its four chains and a pK_2 above 8.0 that provides a role as a headgroup proton trap for oxidative phosphorylation [50]. In eukaryotes CL is synthesised in the mitochondrion, where it remains throughout the life of the cell. During the isolation of proteins from the mitochondrion, CL has been shown to co-isolate with each of the proteins that participate in oxidative phosphorylation. Its headgroup is a high capacity buffer that restricts the amount of pumped protons in the bulk phase water. Thus, the important bioenergetic function of trapping protons by CL may be to simply supply a high buffering capacity to the membrane–water interface. In this way CL bridges the gap between proton source and proton consumer with highly mobile CL monomers or oligomers. Here mobile CLs would laterally shuttle protons from oxidative phosphorylation complexes to the ATP synthase [50]. These specific suggestions of the peculiar properties of CL and its important role in energy conversion were recently supported by experiments on BR in the purple membrane. The glycocardiolipin content does not significantly affect the photocycle (M-intermediate rise and decay) as well as proton pumping of BR. However, interaction of the pumped proton with the membrane surface and its equilibration with the aqueous bulk phase are altered. At reduced GlyCL content the protons are retained at the membrane surface for a shorter time as compared to the "normal" purple membrane, i.e. they are released faster [51].

2.2. Light-induced modulation of protein dynamics during the working cycle of a membrane protein

The proper functioning of a protein requires not only a well-defined three-dimensional structure, but also certain flexibility on fast time scales. Knowledge about the dynamical properties of a protein is of essential importance for understanding the structure–dynamics–function relationships at the atomic level. So far, however, the correlation between internal protein dynamics and functionality has only been studied indirectly in steady-state experiments by variation of external parameters [43,52–56]. To gain access to possible modulations in protein dynamics during its functioning we devised a novel laser-neutron pump-probe experiment which combines in-situ optical activation of the biological function in the membrane protein BR with a time-dependent monitoring of the protein dynamics using quasielastic neutron scattering (QENS) [57,58].

External parameters like temperature or hydration are influencing or restricting the functionality of proteins, like proton translocation in bacteriorhodopsin [33], ligand binding to myoglobin (see, e.g., [59]), and photosynthetic electron transfer in plant photosystem II [60]. In these cases, the temperature-dependent efficiencies of functional processes are found to be correlated with the so-called "dynamical transition" [61] of the respective proteins. This transition represents the onset of localised diffusive protein motions on the picosecond

time scale at temperatures above 200 K, i.e. the onset of internal stochastic structural fluctuations such as diffusive reorientations of methyl groups or other small molecular subgroups [62]. These changes in protein dynamics can be directly investigated using quasielastic neutron scattering (QENS) because of the high incoherent scattering cross section of hydrogen atoms and their almost homogeneous distribution in biomolecules. In the case of BR, steady-state QENS experiments in the dark have established that picosecond diffusive protein motions are indeed suppressed below a temperature of 230 K and at hydration levels lower than 70% r.h. (see e.g. [43,63,64]). This means that protein flexibility may act as "lubricating grease" for the large-scale structural changes in the M-intermediate of BR.

To investigate, if the structural changes are paralleled or even facilitated by modulations in the protein dynamics we performed time-resolved QENS experiments on the light-driven proton pump bacteriorhodopsin embedded the purple membrane (PM) of *Halobacterium salinarum* [57]. BR is activated by absorption of a light quantum, which initiates a photocycle of well-defined protein-chromophore conformations (intermediates) characterised by specific absorption maxima and decay times ranging from 500 fs to about 15 ms in aqueous solution [57,58]. The structural changes accompanying the proton transport are most pronounced in the M-intermediate [65,66]. It is widely accepted that these structural modifications are a prerequisite for the vectorial character of the proton translocation.

QENS experiments were performed at the time-of-flight spectrometer NEAT (Helmholtz Zentrum Berlin, Germany) by synchronising repetitive laser illumination of the sample with a pulsed QENS measurement. In this approach, QENS spectra resulting from individual neutron probe pulses reflect the protein dynamics of specific intermediate states provided that suitable delays between laser excitation and neutron probe pulses are chosen. The chosen spectrometer setup with neutron pulse width of 30 μs and energy resolution of 95 μeV provides access to diffusive protein motions with relaxation times shorter than 20 ps.

A light-induced QENS spectrum of PM was obtained selecting two instants of the neutron pulses during the presence of the M-intermediate of BR upon laser illumination. A comparison to the PM spectrum measured in the dark shows a statistically significant deviation in both, the quasi- and inelastic part, of the QENS spectrum. An analysis of the quasielastic region of the measured QENS spectra in the BR ground state and in the M-intermediate reveals, that the ground state spectrum can be adequately fitted with a phenomenological structure factor comprising of two components with correlation times of 1 ps and 12 ps, respectively, the latter with the dominant amplitude. The true M-intermediate QENS spectrum can be described with only one structure factor with a correlation time of 1 ps. In the experiment the effect of light excitation on protein dynamics is probed for wild-type BR in real time at room temperature under almost physiological conditions. This approach has led to the unambiguous identification of an increase of fast diffusive protein motions and of a significantly larger vibrational mean square displacement correlated with the structural changes in the M-intermediate of BR. This means that the excitation energy gained from the light quantum absorbed locally at the chromophore has been converted into a general softening of the BR protein. It is thus attractive to assume that light excitation induces a softer environment as a prerequisite to overcome potential barriers during the large-scale structural changes in the M-intermediate of wild-type BR [57,58]. Once the temporary softening decays, the structural transition becomes irreversible ensuring a unidirectional proton transport. Functionally important modulations of protein dynamics demonstrated for the first time for the membrane protein BR may be of relevance for other proteins exhibiting conformational transitions in the time course of functional operation. The developed approach is applicable to all photoactive proteins and all enzymatic systems activated by photolysis of caged compounds. In any case, the transient alteration of protein dynamics is a direct proof for the functional significance of protein conformational flexibility.

2.3. Localisation of coenzyme Q_{10} and squalane in the center of the membrane

Redox-active quinones with long polyisoprenoid chains like coenzyme Q are ubiquitous in eukaryotes. They fulfil two established functions as electron/proton carriers in bioenergetic membranes and supercomplexes as well as antioxidants. Since all of the organelle membranes that contain them are exposed to H^+ gradients, coenzyme Q and other polyisoprenes may also serve as inhibitors of H^+ leakage [67]. Squalene, a polyisoprene that is best known as a critical precursor for cholesterol, is present in the membranes of alkaliphiles [68] which are especially sensitive to proton leaks. The localisation of ubiquinone (CoQ_{10}) within membranes has been the subject of many studies [69,70], which have concluded with differing and often conflicting interpretations. Seeking unambiguous evidence for the localisation of squalene and ubiquinone in membranes or lipid bilayers, we employed neutron diffraction [71,72].

Neutron diffraction is an ideal and the most direct tool for localising molecular building blocks in lipid bilayers. Due to the large difference in the coherent scattering length b of a proton ($b_H = -3.74$ fm) and a deuteron ($b_D = +6.67$ fm), an ideally isomorphous replacement can be achieved. We have exploited the contrast variation in two ways: in one, the method is applied in which the membrane constituent CoQ_{10} is protonated and the bilayer lipids are deuterated [72]. In the second experiment we incorporated perdeuterated or protonated squalane, an isosteric analogue of squalene, into stacked bilayers of protonated lipids [71].

Using this approach we found that CoQ_{10} is resident in the center of perdeuterated dimyristoyl phosphatidyl choline (DMPC) bilayers doped with 5 mol% dimyristoyl phosphatidyl serine (DMPS) containing perdeuterated chains (Fig. 2). By determining the difference scattering lenght density between membrane profiles of samples with perdeuterated or protonated squalane in dioleoyl phosphatidyl

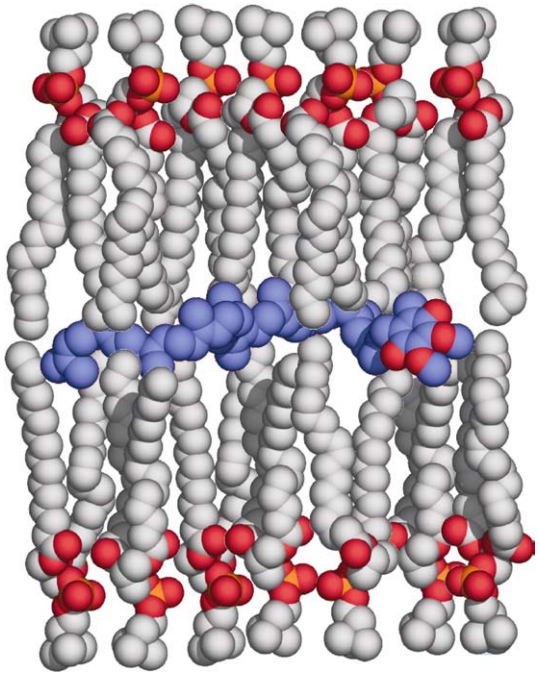

Fig. 2. An artist view of the lipid membrane with embedded ubiquinone derived from the neutron scattering density profiles. The ubiquinone molecule (blue) is sandwiched between the two lipid layers of the membrane. Its conformation is not necessarily straight but its location is confined parallel to the membrane plane with only little intrusions into the lipid acyl chains. Adapted from [72].

choline (DOPC) doped with dioleoyl phosphatidyl glycerol (DOPG) to simulate the negative charges found on natural membranes, we were able to determine the position of squalane in the center of the lipid membrane, quite similar to the polyisoprene chain of CoQ_{10} (Fig. 2).

Two features of straight-chain lipid bilayers seem to provoke the isoprenes to reside in the bilayer center. First, the cooperative motions of the chains in each monolayer are disrupted by intrusion of branched hydrocarbons within that monolayer. Second, the two monolayers are uncoupled so that the lateral cooperative motions of the phospholipid acyl chains within one monolayer do not affect the motions of the other.

CoQ is best known as a carrier of electrons and protons in mitochondria during oxidative phosphorylation as is the ubiquinone analogue plastoquinone in chloroplasts during photophosphorylation. As part of the mitochondrial electron transport chain CoQ transfers electrons from Complexes I and II to Complex III, all embedded in the inner mitochondrial membrane. To facilitate electron transport, CoQ should be freely diffusing in its membrane environment, according to the "random-collision model" of energy conversion [73,74], to encounter the binding pockets in the protein complexes involved [69,75]; this is best if CoQ_{10} resides in the membrane midplane, as shown by our investigation.

Our data prove that the polyisoprene domain of ubiquinone [72], like that of squalane [71], lies in the lipid bilayer center parallel to the membrane plane. Thus long polyisoprenes and polyisopranes can be assumed to have such a residence. Long polyisoprenes include tocopherol, dolichol, plastoquinone, carotenes, and lycopene. The presence of these polyisoprenes in the bilayer center raises a question as to the area occupied by them since they appear to be restricted to the cleavage plane. Each CoQ_{10} occupies the area of about 8 lipid molecules. Thus 6 mol% of CoQ_{10} is sufficient to provide a full surface coverage of each monolayer for the total lipids of the bilayer. The concentration of ubiquinone in biological membranes is largest in mitochondria. Using published data with up to 7 nmol CoQ per mg protein [76], the surface coverage in mitochondria membranes lies between 10% and 30%. Such a calculation suggests that CoQ_{10} can represent a serious barrier for, e.g., proton diffusion across the bilayer of, say, the inner membrane of the mitochondrion. Taken this together with our localisation of both squalane and ubiquinone in the bilayer center, suggests, in accordance with the "water cluster" mechanism for proton leakage [67], that these polyisoprenes may inhibit proton leakage. Such inhibition would be another biological function for them, in addition to their role in redox systems as electron/proton carriers and as antioxidants.

2.4. Isolation of photosynthetic ATP synthases and their subcomplexes

In contrast to BR, many other energy-converting membrane proteins consist of a number of protein subunits and are more challenging in isolation. A comprehensive survey to identify the ideal detergent for solubilisation and the appropriate method of purification is necessary. In case of the ATP synthase, the method has to be adapted to the requirements of the hydrophilic portion (called CF_1 for photosynthetic ATP synthases) and the membrane integral portion (CF_O). Our approaches to gain an ATP synthase sample for diverse functional and structural studies included conventional techniques (density gradient centrifugation and chromatography) but also aimed in optimising alternative purification strategies (preparative electrophoresis).

To separate efficiently Rubisco and other contaminants from the spinach chloroplast ATP synthase, gel filtration or anion exchange perfusion chromatography were applied in presence of the detergents CHAPS and n-dodecyl β-D maltoside [77]. The screening focussed not only on the purity but also on the intactness of the ATP synthase via determination of the ATP synthesis activity driven by an artificial electrochemical proton gradient. The highest purity and activity were achieved by anion exchange chromatography for the detergent DDM and by gel filtration for the detergent CHAPS. In contrast, the detergent Triton X-100, which is frequently used to solubilise CF_1F_O, was found to be inadequate to stabilise the ATP synthase during chromatography [77]. An alternative chromatographic approach – dye–ligand chromatography – can provide a very selective and cost-efficient way of purification if only the ideal dye for a specific enzyme-detergent mixture is identified. To obtain a highly pure and active spinach chloroplast ATP synthase in the presence of n-dodecyl β-D maltoside, a column with the dye Reactive red 120 turned out to be optimal [78]. Alternatively, Reactive green 5 supplies a similar pure ATP synthase sample in the presence of CHAPS.

Upon switching from spinach to the green algae *Chlamydomonas reinhardtii* and even to the thermophilic cyanobacterium *Thermosynechococcus elongatus*, the purification method for the ATP synthase had to be adapted. The single chromatographic steps that yielded highly pure spinach CF_1F_O only supplied a core ATP synthase sample with many contaminants for the alga [79]. In face of the purity issues, the intactness of the oligomer III_x in this chloroplast ATP synthase was assured as important basis for subsequent studies. To isolate the intact ATP synthase holoenzyme of *T. elongatus* a combination of dye–ligand and ion-exchange chromatography was needed [80].

To reveal the proton-to-ATP ratio via structural studies, not the complete ATP synthase is required but only the proton-driven rotor c_x or III_x has to be maintained as native oligomer. The high stability of this oligomer in presence of strong detergents or other denaturants was the prerequisite for a successful isolation. For the spinach chloroplast ATP synthase, the oligomer of subunit III proved to be stable in SDS [81,82] allowing its purification based on density gradient centrifugation [83,84]. Other groups developed a strategy for spinach III_X using lauroyl sarcosine [85–87]. This detergent was introduced to isolate the c_{11} oligomers from *Ilyobacter tartaricus* [88] as requirement to solve its crystal structure [89] but proved to be a unique tool for diverse organisms. By sodium thiocyanate treatment of the spinach chloroplast ATP synthase the preparation of CF_O, containing the proton-driven rotor III_{14} and the membrane integral parts of the stator (subunits I, II and IV), succeeded [90].

Our alternative purification strategy for the ATP synthase applied preparative native electrophoresis [91–94]. The introduction of the so-called blue-native electrophoresis or BN-PAGE [95] made the analysis of protein complexes feasible for many applications. The binding of the anionic dye Coomassie Brilliant Blue G-250 (CBBG-250) to protein species confers a negative charge required for electrophoretic separation and diminishes artificial aggregation as the main problem for membrane proteins. BN-PAGE permits isolation of functional CF_1F_O directly from solubilised spinach thylakoids in one step [94]. Using a cathode buffer with low CBBG-250 concentration (0.002%), CF_1F_O remains intact. An increase of the CBBG-250 concentration in the cathode buffer up to 0.02% (as described in the original BN-PAGE protocol [95]) disassembles the ATP synthase, allowing an isolation of both parts, CF_O and CF_1, separately. The subsequent electro-elution of the respective bands from the gel enables almost quantitative recovery of CF_1F_O, CF_O, and CF_1. Although CBBG-250 neither abolishes the catalytic activity of the isolated CF_1F_O and CF_1 nor affects the subunit composition and the high α-helical content of CF_O [96], the strong blue colour of samples from preparative BN-PAGE can disturb biophysical investigations. In this case, it is recommended to remove most of CBBG-250 using gel filtration and replace the dye by the detergent CHAPS [96].

2.5. Properties of the chloroplast ATP synthase

Isolated subunits or their oligomers can provide useful pieces of information by diverse biophysical techniques that have to be assembled to reveal new insights into a sophisticated enzyme complex (see also Section 2.6). By Fourier-transform infrared and

circular dichroism spectroscopy, the predominantly α-helical secondary structure of subunit III was demonstrated [84]. For monomeric subunit III, a conformational change was observed when diluting the SDS-solubilised protein. Under the same conditions the conformation of the oligomer III_X did not change. MALDI mass spectrometry provides additional information of native proteins, e.g. the determination of the mass for the monomeric subunit III (8003 Da) demonstrated that no posttranslational modifications occurred [84].

During the catalytic function of the ATP synthase, tension generated by the rotational torque is compensated by the stator (e.g. [97]). For this task, a peripheral stalk flexibly fixes the hydrophilic catalytic part F_1 to the membrane integral proton-conducting part F_O of the ATP synthase [98]. While in bacteria a homo-dimer of b subunits forms the peripheral stalk, plant chloroplasts and cyanobacteria possess a heterodimer of subunits I and II. To better understand the functional and structural consequences of this unique feature of photosynthetic ATP synthases, a procedure was developed to purify subunit I from spinach chloroplasts [99]. The secondary structure of subunit I, which is not homologous to bacterial b subunits, was compared to heterologously expressed subunit II using CD and FTIR spectroscopy. The content of α-helix was determined by CD spectroscopy to 67% for subunit I and 41% for subunit II. In addition, bioinformatics was applied to predict the secondary structure of the two subunits and the location of the putative coiled-coil dimerisation regions. Three helical domains were predicted for subunit I and only two non-interrupted domains for the shorter subunit II. The predicted length of coiled-coil regions varied between different species and between subunits I and II [99].

In spinach chloroplasts, the central stalk (subunits γ, ε) forms the rotor with the cylinder of subunits III and transmits proton-motive force from F_O to F_1, inducing conformational changes of the catalytic centers in F_1. The ε subunit is an important regulator affecting adjacent subunits as well as the activity of the whole protein complex. Using a combination of chemical cross-linking and mass spectrometry, we monitored interactions of subunit ε in spinach chloroplast ATP synthase with III and γ [100]. One cross-link defined the distance between ε-Cys6 and III-Lys48 to be 9.4 Å at minimum. ε-Cys6 was competitively cross-linked with subunit γ. Altered cross-linking yields revealed the impact of nucleotides and Mg^{2+} on cross-linking of subunit ε. The presence of nucleotides apparently induced a displacement of the N-terminus of subunit ε, which separated ε-Cys6 from both III-Lys48 and subunit γ, and thus decreased the yield of the cross-linked subunits ε and γ as well as ε and III. This change may contribute to the change at the ε C-terminus from a closed to an open conformation leading to inhibition of ATP hydrolysis. However, increasing concentrations of the cofactor Mg^{2+} favoured cross-linking of ε-Cys6 with subunit γ instead of III-Lys48 indicating an approximation of subunits γ and ε and a separation from III-Lys48 [100]. The influence of free magnesium on the yield of ε-III crosslinks is an indication for a Mg^{2+} dependent control of proton conductance since the N-terminus of ε seems to be responsible for the ability of subunit ε to block proton conductance [101]. Additionally, for rat liver mitochondria [102] and spinach chloroplast ATP synthase [103] the presence of 1–2 mM free magnesium cations significantly inhibited the ion conductance of the membrane integral part of the ATP synthase.

2.6. The proton-to-ATP stoichiometry of chloroplast ATP synthases

The interaction of the subunit IV with the oligomer of subunit III facilitates the transport of protons through the CF_O part of the chloroplast ATP synthase. In current models of ATP synthases, the proton-to-ATP ratio and therefore the efficiency of energy conversion is directly determined by the number of proton-transporting subunits (or protomers: protein monomers) of the rotary oligomer III_x. Previously it was believed that the stoichiometry would be 9 or 12 resulting in an integer proton-to-ATP ratio, i.e. 3 or 4 protons per ATP. To determine the stoichiometry of subunit III in spinach chloroplasts we reconstituted the complete CF_1F_O or suitable subcomplexes (see Section 2.4) into lipid bilayers for the subsequent structural analysis by electron and atomic force microscopy.

Upon adsorbing CF_1F_O liposomes on a mica surface for atomic force microscopy, they spread and form planar lipid bilayers [104]. To reveal the details of the membrane integral part, the CF_1 part can be removed either by application of a chemical denaturant or less efficiently by using the AFM tip as a nanotool for mechanical stripping. In fact, the latter procedure was one of first reported nano-manipulations of biomolecules by the AFM. This approach allowed observation of ring-like protein structures with a central dimple in the lipid bilayer which possess an outer diameter of approx. 7 nm [104]. By utilising CF_O isolated via preparative BN-PAGE as starting material for reconstitution into lipid membranes, similar structures were monitored by electron microscopy [96]. With a mean diameter of 6.7 nm not only the shape but also the size was similar to that of earlier observations [104], which confirms the importance of these rings as integral building blocks of CF_O.

These promising preliminary results build a base for a high-resolution structure analysis. By SDS treatment of the ATP synthase and density gradient centrifugation, the homo-oligomer III was isolated. Imaging the topography of the densely packed subunit III oligomers by contact-mode atomic force microscopy revealed alternating ring-like structures of two different diameters (panel A of Fig. 3) [83]. The narrow and the wider rings of the subunit III oligomers have outer diameters of 5.9 ± 0.3 nm and 7.4 ± 0.3 nm, respectively. Both orifices have inner diameters of 3.5 ± 0.3 nm. Directly from the recorded images, 14 subunits per oligomer can be counted in most cases (see Fig. 3). An analysis of angular power spectra from 320 individual images of well-preserved particles confirmed this result, and yielded a distinct single peak at 14-fold symmetry [83].

Although the AFM topographies demonstrated clearly the III_{14} stoichiometry, utilisation of the harsh detergent SDS during isolation raised the question if the observed association of subunits is really the native oligomeric ring structure of the chloroplast ATP synthase [105–107]. Therefore, three fundamentally different chloroplast ATP synthase samples of increasing complexity were visualised by atomic force microscopy [90]. The samples are distinguishable in respect to the isolation technique, the detergent employed, and the final subunit composition. The homo-oligomer III was isolated as described before (Fig. 3A), the proton-turbine III + IV was obtained by blue-native electrophoresis (Fig. 3B), and complete CF_O was isolated by anion exchange chromatography of NaSCN splitted ATP synthase (Fig. 3C). In all three ATP synthase subcomplexes 14 and only 14 circularly arranged subunits III composed the intact transmembrane rotor. Interestingly, a correlation between the presence of subunit IV in the imaged sample and the appearance of a central protrusion in the narrower orifice of the oligomeric cylinder III_{14} has been observed. In contrast to current predictions, in chloroplast F_O the subunit IV can be found inside the cylinder III_{14} and not at its periphery, at least in the reconstituted 2D arrays imaged [90].

In addition to atomic force microscopy, 2D aggregates are also appropriate for a high-resolution study by electron microscopy [108]. Based on screening various negatively stained specimens, the best ones were selected for cryo-electron microscopy. These 2D crystals were obtained by reconstitution of the proton-turbine III+IV from BN-PAGE. Unfortunately, strong stacking of several layers occurred which hampered the analysis of the electron micrographs (Fig. 3D). Upon processing the images, an electron density map showing the α-helices was created (Fig. 3E). Determination of the number of single subunits III belonging to an oligomer required identification of densities from one specific layer. By highlighting these densities and including the fact, that each subunit III consists of two α-helices, the III_{14} stoichiometry can be recognised easily. The hairpins of helices of a

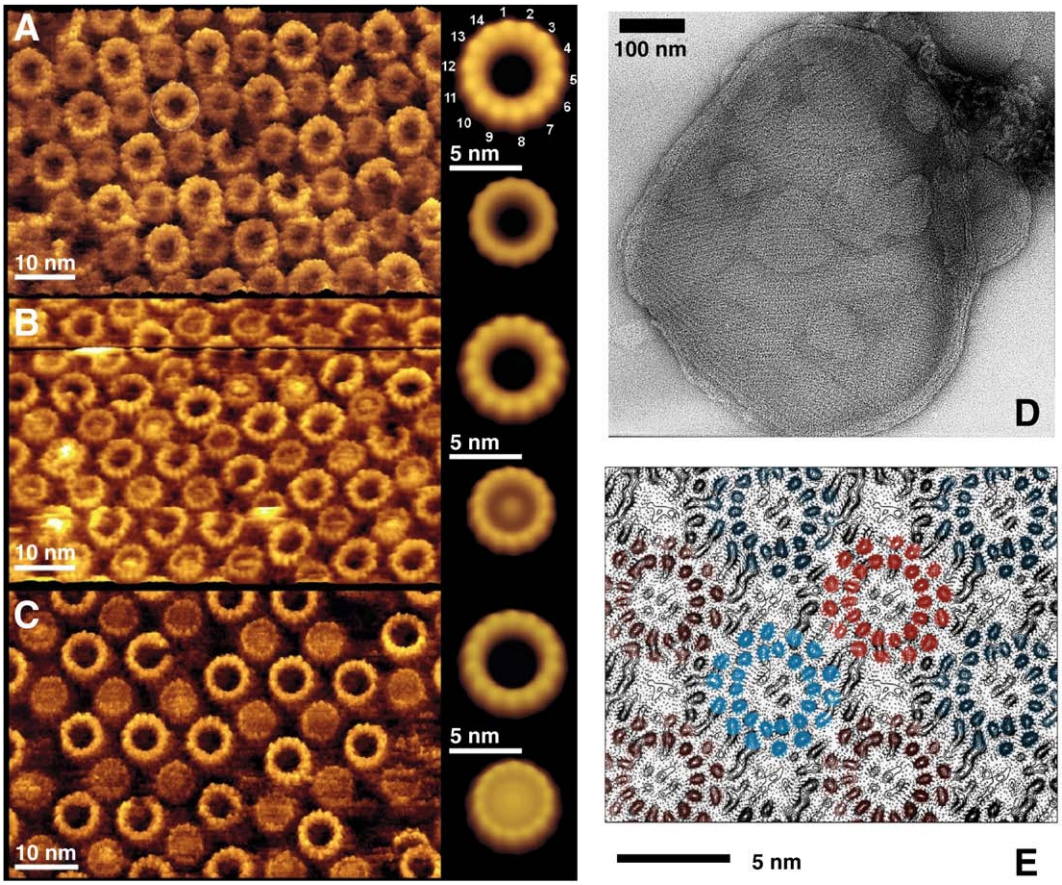

Fig. 3. 2D-arrays showing the III_{14} stoichiometry of the spinach chloroplast ATP synthase. In panels A–C atomic force micrographs are depicted from samples with increasing complexity imaged by contact-mode AFM (from [90]). (A) Homo-oligomer III_{14}; (B) the proton-turbine $III_{14}IV$; and (C), CF_O; the right panel displays averaged and symmetrised topographs of the wide and narrow oligomer ends. (D) Electron micrograph of negatively stained multilayer crystals with homo-oligomer III_{14} and subunit IV. (E) Electron density map of approximately 8 Å resolution from cryo-electron micrographs (JEOL 3000 SFF) showing the α-helices of the III_{14}–IV-crystals.

subunit III monomer are arranged in such a way that a smaller inner ring of 14 α-helices is surrounded by an outer ring of 14 α-helices (blue or red coloured in Fig. 3E). The four to five densities inside the ring could represent the predicted helices of subunit IV, however, contribution by the density of a stacked second membrane layer cannot be excluded. The stoichiometry of 14 observed by AFM is confirmed by electron microscopy and moreover recently by another group [86]. In spite of the clear demonstration that III_{14} is not a biochemical artefact, there is still a lack of agreement with functional data of proton translocation through the ATP synthase [109,110].

Accumulating structural data suggests that the number of identical subunits (III or c) assembled into the cation-powered rotor of ATP synthases depends on the biological origin (e.g. [29,83,85,87,89,90,111–114]). The stoichiometries identified vary from 10 in yeast mitochondria [29] or *Escherichia coli* and *Bacillus* PS 3 [105,115], 11 in Na^+-ATP synthases [88,89,111–113], 12 in a prokaryotic V-ATPase of *Thermus thermophilus* [114], 13 in thermoalkaliphilic *Bacillus* sp. strain TA2.A1 [116], up to the range of 13 to 15 in cyanobacteria [85,87]. This remarkable range raises the question of the principle behind the different stoichiometries. According to the chemi-osmotic theory the driving forces of the electrochemical proton gradient, i.e. membrane potential $\Delta\psi$ and pH gradient ΔpH, are equivalent [3]. For the chloroplast ATP synthase, ΔpH is the main component [117], but $\Delta\psi$ has an important function for storage of proton-motive force [118]. In contrast, $\Delta\psi$ predominates as driving force for the mitochondrial ATP synthase. Therefore, an adaptation of the stoichiometry to the specific component of the proton-motive force is considerable. In this context, the equivalence of $\Delta\psi$ and ΔpH is discussed controversially (e.g. [114,119]). The demonstration of $\Delta\psi$ to be obligatorily required for ATP synthesis suggests that the membrane potential is the main driving force for the rotation of the oligomer [120]. Therefore, the components of the proton-motive force are kinetically not equivalent [119] and different sizes of the cation-powered rotors may be nature's solution to cope with the challenges of diverse environments.

The problem "what dictates the size of a ring?" [121] still has to be resolved unambiguously. In AFM images of the cylindrical transmembrane rotors from spinach chloroplasts and from *I. tartaricus* occasionally individual rotors exhibit gaps of the size of one or more subunits (Fig. 3A–C) [122]. Complete rotors and arch-shaped fragments of incomplete rotors revealed the same diameter within one ATP synthase species. These results suggest the rotor diameter and stoichiometry to be determined by the shape of the subunits and their nearest neighbour interactions [122]. An observed self-assembly of subunits to an oligomer confirms that an intrinsic feature of subunit c (or III) determines the stoichiometry [123]. Alternatively, a specific cofactor like the UncI protein could play a chaperone-like role to assist the oligomer assembly [124,125].

In context with parameters affecting the number of subunits in the oligomer and therefore the diameter of the ring, it is controversial if the stoichiometry is affected by the metabolic state of any organism. For *E. coli*, data were published indicating that different carbon sources during cultivation lead to different ratios (subunit c compared to subunit b) assembled into the ATP synthase [126,127]. We examined a possible alterability of the stoichiometry caused by the metabolic state of *C. reinhardtii* [79]. To distinguish oligomers with different stoichiometries, a gradient gel system was established. Several growth parameters, i.e., light intensity, pH value, carbon

source, and CO_2 concentration, were varied to determine their effects on the stoichiometry. Contrary to the previous suggestions, the oligomer III of the chloroplast H^+-ATP synthase always consists of a constant number of monomers over a wide range of metabolic states. Recently, a constant stoichiometry of the oligomer was confirmed for Na^+-ATP synthases [113,128]. Even for the H^+-ATP synthase of *E. coli* new data [129] affirm our previous finding of a constant number of subunits [79].

2.7. Supramolecular architecture of chloroplast ATP synthases

In one and the same plant cell, two significantly distinct H^+-ATP synthases are housed in separate organelles. One major difference between mitochondrial and chloroplast ATP synthases is the amino acid sequence of comparable polypeptide chains. Moreover, the subunit composition of plant mitochondrial ATP synthase resembles more that of other mitochondrial homologues, even if additional (and novel) subunits were present, as demonstrated e.g. for algae [130]. In proteomic studies of the green algae *C. reinhardtii* employing BN-PAGE, the organisation of ATP synthases appeared to be different. For the mitochondrial ATP synthase, an extraordinarily stable dimeric arrangement was observed [131] and confirmed by our own experiments [132]. In fact, mitochondrial ATP synthase dimers and even oligomers are found in essentially all eukaryotes investigated by this approach so far (reviewed by [133–135]; see Section 2.8). In contrast, the chloroplast CF_1F_O was previously assumed to exist solely as a monomer and dimerisation was proposed to be a unique feature of the mitochondrion [133]. All single steps of an isolation procedure, especially the treatment of cells, affect protein stability and have to be considered. One important aspect is the sensitivity of membrane protein complexes like CF_1F_O against mechanical stress in respect to enzymatic activity and structural integrity [136]. Additionally, all buffer components (e.g. detergents and salts) affect fragile protein–protein interactions. Upon using the mild detergent digitonin and reducing the pressure during disruption of cells, we were able to identify dimers of the chloroplast ATP synthase in *C. reinhardtii* via BN-PAGE [137]. These chloroplast ATP synthase dimers dissociate into monomers upon incubation with vanadate or phosphate but not by incubation with molybdate, while the mitochondrial dimer is not affected by this treatment. Therefore, a distinct dimerisation mechanism for mitochondrial and chloroplast ATP synthase is suggested. Since vanadate and phosphate bind to the active sites, contact sites facilitating dimerisation are presumably located on the hydrophilic CF_1 part as compared to significance of the F_O portion in mitochondrial ATP synthase dimers.

The dissociation of chloroplast ATP synthase dimers at elevated phosphate concentration suggests a regulation by cell physiological processes. Particularly, different growth conditions affect the metabolism. *C. reinhardtii* is able to utilise different sources of energy generation. Besides photosynthesis (photoautotrophic growth) the alga is able to metabolise organic substrates such as acetate for heterotrophic nutrition, or both at the same time (photomixotrophic growth). We applied two different growth conditions, photomixotrophic and photoautotrophic growth, and studied the influence on the metabolic state of the cell by BN-PAGE combined with mass spectrometry [132]. Cells grow faster in the presence of acetate, they contain more protein per cell, and the composition of photosynthetic supercomplexes change.

To establish a reliable quantitative method, stable isotope labelling was applied to monitor changes in assembly and disintegration of protein complexes and supercomplexes [138]. As experimental basis, *C. reinhardtii* cells were cultivated at the two different growth conditions and analysed on BN gels upon solubilisation with digitonin. On the one hand, cells from two separate cell culture conditions were independently applied to gels and the monomer/dimer ratio of CF_1F_O were quantified from Coomassie stained gel bands. On the other hand, stable isotope labelling of living organisms was employed. Here, ^{14}N and ^{15}N labelled algae from two culture conditions were combined before harvesting and the amount of ATP synthase monomer and dimer was quantified by mass spectrometry. Photoautotrophical algae cultures were grown in the presence of ^{15}N and photomixotrophical cells at natural ^{14}N abundance, respectively. As compared to photoautotrophic growth, an increased assembly of ATP synthase dimers at the expense of pre-existing monomers during photomixotrophic growth was observed, demonstrating a metabolic control of the dimerisation process [138]. In contrast, although the abundance of mitochondrial ATP synthase increased during photomixotrophic growth, only its dimer is present. Such dimers of the mitochondrial ATP synthase as well as supramolecular protein assemblies of respiratory chain complexes were identified not only in algae but in a wide range of organism.

2.8. Supramolecular organisation of mitochondrial respiratory chains

Using BN- and CN-PAGE after gentle solubilisation of isolated mitochondria [92,93], it could be demonstrated that the respirasome organisation of bovine heart respiratory complexes I, III, and IV as well as F_1F_O-ATP synthase dimerisation (reviewed in [133–135]) are also found in rats [139,140]. In corresponding studies, respirasome-like supercomplexes were detected in various eukaryotes, particularly the filamentous fungi *Podospora anserina* [141,142] and *Neurospora crassa* [143] as well as in green, photosynthetically active tissues of higher plants [144]. Strikingly, analysing mitochondria isolated from fresh or short-term stored bovine heart tissue, significantly higher amounts of respiratory supercomplexes $I_1III_2IV_{1-4}$ and ATP synthase dimers than reported before were recovered. Even supercomplexes $I_xIII_yIV_z$ with higher apparent masses than that of $I_1III_2IV_4$ as well as higher oligomers of ATP synthase were found [93,135,139,145]. The application of CN-PAGE retained nearly all of the bovine heart complexes I, III, and IV as supercomplexes and ~80% of total ATP synthase as dimers and higher oligomers [139]. These results support the hypothesis of supramolecular networks of the respiratory chain and ATP synthases (reviewed in [133–135]). Accordingly, the quality and the way of processing of the starting material is of major importance to get optimal yields of OXPHOS supercomplexes as outlined [93,135] like in case of CF_1F_O dimers from *C. reinhardtii* [137] (see Section 2.7). This shows that susceptible supramolecular assemblies of membrane protein complexes might easily escape detection applying biochemical methods like detergent treatment and native gel electrophoresis.

Those studies comparing mitochondria from a variety of eukaryotes revealed apparent peculiarities of the supramolecular organisation of the respiratory chain (reviewed in [135]). Most importantly, complex I dimers could be clearly shown so far only in filamentous fungi, whether complexes III and IV are present or not [141,142] and also in case of the three *N. crassa* mutants nuo21, nuo29.9, and nuo51 that assemble a “complete” complex I but missing each one subunit [143]. It is conceivable that complex I dimers exist also in other eukaryotes but sufficient evidence is still lacking [135]. As an intriguing feature of the fungal respiratory chain, even the simultaneous loss of both complexes III and IV has no detrimental effects on assembly/stability and activity of fungal complex I [142] in contrast to the situation in mammals (see Section 2.9). The respective *P. anserina* mutants *Cyc1-1,Cox5::ble* and *Cyc1-1,Cox5::ble(Gpd-Aox)* are the first obligatorily aerobic eukaryotic strains with a functional complex I but an artificial lack of both respiratory complexes III and IV [142]. Fungal-specific features not found in mammals are discussed that must be responsible for assembly/stabilisation of fungal complex I when complexes III and IV are absent such as the presence of the alternative oxidase (AOX), bypassing complexes III and IV, and complex I dimerisation [142]. Nonetheless, whenever the conditions for assembly of complexes III and IV are in place, they seem to be involved in assembly/stabilisation of fungal complex I [142]. Particularly, wild-

type-like amounts of I–III–IV supercomplexes could be found in the *N. crassa* mutant nuo51 whose complex I is inactive due to lack of the NADH-binding 51-kDa subunit. These supercomplexes are the first example of respirasomes without overall NADH oxidase (I–III–IV) activity ("inactive" respirasomes) in any organism only able to oxidize ubiquinol by molecular oxygen (ubiquinol oxidase, III–IV) [143], demonstrating that respiratory supercomplexes have also major nonrespiratory significance and cannot be solely related to conceivable enzymatic advantages such as substrate channelling ([135]; see Section 2.9).

In summary, there are important advances in our knowledge of OXPHOS supercomplexes including the determination of single particle structures (see Section 2.9). However, major research efforts using various approaches are still needed over the next years. In particular, it is mandatory to unravel the biogenesis of complex I as well as the true supramolecular organisation of the respiratory chain in the inner mitochondrial membrane and its precise functional significance in a variety of model eukaryotes [142].

2.9. Supramolecular architecture of OXPHOS membrane protein complexes

To structurally characterise the supercomplexes I_1III_2 (consisting of one complex I and a dimer of complex III; 1500 kDa) and $I_1III_2IV_1$ (with one additional complex IV; 1700 kDa), bovine heart mitochondria were solubilised with digitonin, separated by BN-PAGE and electro-eluted [146]. The composition of both isolated supercomplexes was confirmed by peptide mass fingerprinting. The enzymatic activity of each supercomplex component was tested to confirm their functional integrity after isolation. In-gel activity staining showed NADH–dehydrogenase activity of complex I in both supercomplexes and cytochrome *c* oxidase activity of complex IV in supercomplex $I_1III_2IV_1$ [146]. For the first time, the activity of two isolated respiratory supercomplexes was quantitated and a pronounced enzymatic advantage of the $I_1III_2IV_1$ respirasome demonstrated. Spectrophotometric activity assays using specific inhibitors were employed to assess NADH:ubiquinone reductase activity of complex I and cytochrome *c* reductase activity of complex III in the electro-eluted samples. Under the conditions used, complex I in supercomplex I_1III_2 displayed only about half the activity of that in supercomplex $I_1III_2IV_1$ (I_1III_2: 0.13 ± 0.04 mU/mg protein; $I_1III_2IV_1$: 0.30 ± 0.11 mU/mg protein). Complex III was active in supercomplex $I_1III_2IV_1$, but supercomplex I_1III_2 showed only minor cytochrome *c* reductase activity (I_1III_2: 0.06 ± 0.02 mU/mg protein; $I_1III_2IV_1$: 0.99 ± 0.28 mU/mg protein [146]). In conclusion, both isolated supercomplexes displayed activity, but supercomplex $I_1III_2IV_1$ was significantly more active.

After purification and demonstration of enzymatic activity, their structures in projection were determined by single particle image analysis (Fig. 4A–E; [146]). Both supercomplexes had two preferred orientations; a 'top' view as seen from the intermembrane space (Fig.

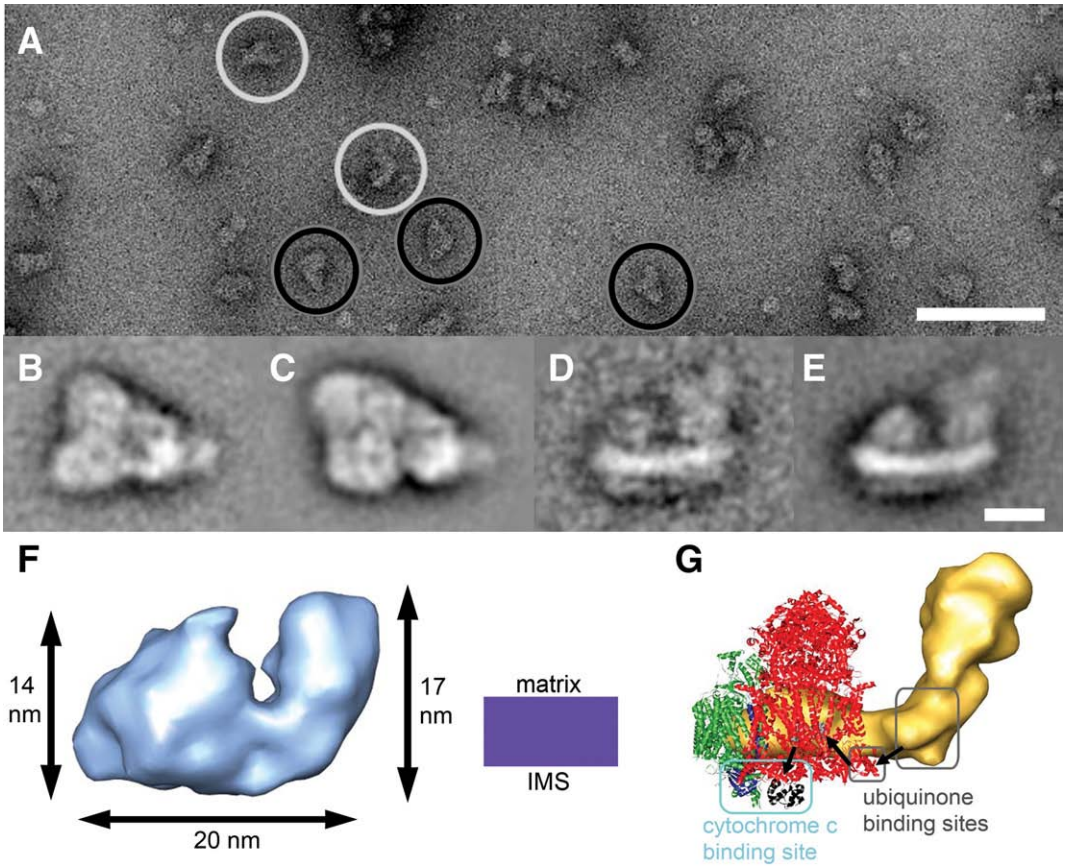

Fig. 4. Structural studies of supercomplexes. (A) Transmission electron microscopic image of the isolated supercomplex $I_1III_2IV_1$. Top views are indicated by black circles and side views by light gray circles. The sample was negatively stained with 1% uranyl acetate. Averaged 2D projection maps of the supercomplexes. Top views (as seen from the intermembrane space) of supercomplex (B) I_1III_2 and (C) $I_1III_2IV_1$. Side views (as seen along the membrane plane) of supercomplex (D) I_1III_2 and (E) $I_1III_2IV_1$. (F) Side view of the 3D map of supercomplex $I_1III_2IV_1$ as seen along the membrane plane. The location of the membrane in the side view is displayed in purple. IMS: intermembrane space. (G) The three individual complexes as they would assemble to form supercomplex $I_1III_2IV_1$. The electron microscopic 3D map of complex I filtered to 5.0 nm [15] is shown in yellow, the X-ray structure of complex III_2 (PDB ID 2A06, [168]) is displayed in red, and the X-ray structure of complex IV (PDB ID 1OCC, [26]) is shown in green. The ubiquinone interaction site in complex I and the interaction site in the complex III dimer are marked in gray. The two cytochrome b_L hemes of the complex III dimer are shown in light gray. The ubiquinone diffuses from its interaction site in complex I to its interaction site in the complex III dimer (black arrows). The cytochrome *c* interaction site in complexes III and IV is marked in light blue. Cytochrome *c* bound to complex III is coloured in black (from 1KYO PDB ID; [169]), and subunit II, which is the cytochrome *c* binding site, from complex IV is displayed in blue. The scale bars represent in (A) 100 nm and (E) for (B–E) in 10 nm. Modified from [146,147].

4B–C) and a 'side' view as seen along the membrane plane (Fig. 4D–E). A difference map between the supercomplexes I_1III_2 and $I_1III_2IV_1$ closely fits the X-ray structure of monomeric complex IV and shows its location in the assembly [146].

In addition, we presented the first 3D map of a respiratory chain supercomplex (Fig. 4F [147]) which gives the first insight into the positions and interactions of the individual respiratory chain complexes when assembled into a supercomplex [147,148]. It was determined by random conical tilt electron microscopy analysis of the bovine supercomplex $I_1III_2IV_1$. Within this 3D map the positions and orientations of all the individual complexes in the supercomplex were determined unambiguously (Fig. 4G). The ubiquinone and cytochrome *c* binding sites of each complex in the supercomplex could be located. One function of the assembly into a supercomplex is the stabilisation of the individual complexes. The assembly and/or stabilisation of mammalian complex I is dependent on supercomplex formation with complex III and/or IV as supported by strong evidence (for references see [135]), whereas this is not essential in fungi ([142]; see Section 2.8). The 3D map of $I_1III_2IV_1$ indeed shows extensive interaction sites at membrane domains of both complexes III_2 and IV with complex I, which keeps it in a stable conformation. The mobile electron carrier (ubiquinone or cytochrome *c*) binding site of one complex is facing and is in proximity to the mobile electron carrier binding site of the succeeding complex of the respiratory chain (Fig. 4G). This arrangement is significant as it results in short diffusion distances for ubiquinone and cytochrome *c*, thus facilitating a more efficient electron transfer from complex I via complex III to complex IV and might reduce the detrimental generation of ROS, participating in ageing as well as degenerative diseases like Alzheimer's and Parkinson's (see Section 2.10). The structural evidence provided for direct substrate channelling in the supercomplex assembly with short diffusion distances for the mobile electron carriers is supported by our enzyme activity determinations.

Detailed knowledge of the architecture of the active supercomplexes is a prerequisite for a deeper understanding of energy conversion by mitochondria in mammals, e.g. do the OXPHOS complexes operate according to the "solid-state", the "random-collision" or the "plasticity" model [73,149].

2.10. Quantitative assessment of membrane proteins and protein complexes based on native gel electrophoresis

Changes in stability and/or activity of respiratory chain complexes, involving the abundance changes in specific subunits is of critical importance for mitochondrial function. We have followed three independent quantitative approaches, post-electrophoretic staining with fluorescent SYPRO® Ruby, pre-electrophoretic covalent labelling of proteins with fluorescent CyDyes and isotope labelling (see Section 2.7), to assess the changes in abundance of OXPHOS complexes, supercomplexes and the respective subunits. Coupling these quantitative methods with BN/CN-SDS gel system facilitates the evaluation of both soluble and membrane proteins, as well as the protein–protein interactions.

Among the range of post-electrophoretic staining methods, the use of fluorescent stains belonging to SYPRO family (Molecular Probes Inc./Invitrogen Inc.) offers the desired sensitivity and high dynamic range of about 10^3. We used the SYPRO Ruby stained images of 2D-BN/SDS PAGE-resolved mitochondrial proteome, to quantify the abundance of individual OXPHOS complexes (I to IV) and of their supercomplexes. The normalisation was routinely done using external standard molecular weight markers, but at times could also be done internally using proteins, which do not change in expression. The staining based quantification method was coupled with Delta2D programme (Decodon), for image analysis and statistical tests. This approach was very effective to monitor simultaneously the relative changes in oligomeric status of OXPHOS complexes and stability of their supercomplexes. Such quantitative evaluation of the dynamic assembly of the OXPHOS machinery, in response to a physiological stimulus could be correlated to changes in activity as visualised by in-gel activity assays using 1D blue-native/colourless native gels [146,150]. For rat cortex mitochondria, an age-dependent decline in the amount of intact ATP synthases (1.2-fold) as well as in the proportion of especially the OXPHOS supercomplexes I_1III_2 (2.4-fold) and $I_1III_2IV_1$ (1.4-fold) was detected by this approach [170]. The proportion of ATP synthase oligomers and of non-attached F_1 is significantly larger in aged mitochondria [150]. These observations elucidate the link between respiration and longevity. On the other hand, in a rat model of early Parkinson's disease, the overall abundances of individual OXPHOS complexes and supercomplexes is not altered, but the activity of a specific supercomplex boosted [151].

There are often few critical subunits, responsible for activity/assembly of the OXPHOS complexes. An insight was obtained for the abundance changes of such critical individual subunits of complex I, IV and V by differential quantitative analysis using the "Difference in Gel Electrophoresis (DIGE)" approach. With this technique, samples differentially labelled with spectrally resolvable fluorescent cyanine dyes Cy2, Cy3 and Cy5 (GE Healthcare) are loaded onto the same gel. Over a >10,000-fold protein concentration range DIGE can reliably detect changes in abundance of a protein of 15% (fold-change minimum of 1.15-fold) [152]. Use of common internal standard (pool of all samples under comparison) for all gels ensures accurate normalisation and allows convenient grouping of multivariate samples, though resolved on different gels. Integrating the fluorescence DIGE technique with BN-PAGE offers a unique opportunity for sensitive evaluation of abundance changes besides protein-protein interactions [153]. Using the BN-DIGE approach we could identify abundance changes in specific subunits of complex I (17.2 kDa and 40.8 kDa) and complex IV (subunits II, Va and VIb) in rat liver mitochondria, indicating a lowered activity of the complexes with calorie restriction, as a mechanism to minimise free radical leak and ROS generation [154]. Structurally associated ATP synthase subunits, the F_1 complex beta subunit and the F_O complex subunit b showed a concomitant decrease in abundance with calorie restriction [154], indicating less assembled monomeric ATP synthase and reduced ATP production in rat liver mitochondria. Differential proteomic profiling of three evolutionary far distant organisms reveals distinct patterns of age-related oxidative changes and the ATP synthase as a major player in ageing [155].

A comprehensive understanding of the structural diversity and dynamic nature of chloroplast and mitochondrial sub-proteomes could be developed by combining the above mentioned quantitative approaches and validating the observations at a functional level. This will lead the interpretation of the proteome beyond mere cataloguing of abundance changes to more "meaningful" information.

2.11. Intercalation of the Alzheimer peptide Aβ and membrane perturbation evidenced by neutron scattering

It has been established that alterations in membranes and resulting changes in bioenergetics are the trigger of severe diseases, such as Morbus Alzheimer and Parkinson, and vice versa. Recent studies indicate that mitochondria are important targets of Amyloid-β peptide (Aβ) [156]. There is increasing evidence that synaptic damage and mitochondrial dysfunction have a significant role in AD development [157]. Aβ is a short polypeptide of 39–43 amino acids considered a trigger agent of Alzheimer's disease (AD). The so-called amyloid hypothesis links the presence of insoluble fibril-like Aβ aggregates to the pathogenesis of the disease [158]. For more than a decade the amyloid hypothesis has been the driving idea in the attempt of understanding the trigger of the neuritic damage leading to dementia. Because of the controversial data collected, no consensus about this theory has been reached to date [159]. Recently, new suppositions

have been put forward and the attention focus now on non-fibrillar soluble forms of monomeric or oligomeric Aβ [160]. The mechanism of action of Aβ continues to remain a mystery. To understand its unknown mechanism of action, also in relationship to a therapeutic treatment of the disease, the interaction of Aβ with the cell membrane has to be elucidated at the molecular level [161,162].

In our studies the interaction of *monomeric* forms of Aβ with lipid membranes was analysed. It was ascertained by neutron diffraction on stacked lipid multilayers that a toxic fragment of Aβ is able to deeply penetrate and perturb the lipid bilayer [161]. The use of a selectively deuterated amino acid (i.e., leucine-34, the penultimate amino acid in the C-terminal region) has allowed us to determine unambiguously the position of the neurotoxic fragment Aβ(25–35) in the membrane. Two populations of the peptide have been detected, one in the aqueous vicinity of the membrane surface and the second inside the hydrophobic core of the lipid membrane. The location of the C-terminus was studied for two different lipid compositions (i.e., POPC and POPC/POPS 92:8 mol/mol) and it was found to be dependent on the surface charge of the membrane. In the anionic POPC/POPS membrane that mimics the composition and negative net charge state of neuritic cell membranes, 54% of Aβ is located in the hydrophobic core, 5.9 Å from the center of the membrane (Fig. 5). In POPC membranes, an even larger amount of the peptide, i.e., 86% is found inside the membrane. However, it does not intercalate as deeply, only to a position corresponding to the polar head groups of the lipids, 14 Å from the center of the membrane [161].

Furthermore, we were able for the first time to prove by neutron diffraction the penetration of Aβ(25–35) and to determine the depth of penetration of the C-terminus in the bilayer core when Aβ(25–35) was externally administered [163]. Externally administered Aβ(25–35) penetrates deeply into the lipid bilayers. This information could provide the structural basis for the channel creating properties of Aβ. By spontaneously penetrating the membrane, it may also interact with integral membrane proteins such as receptors. Our data show in addition that the membrane is severely perturbed by the intercalated Aβ(25–35), as exemplified by the broadening of the scattering density in the headgroup region and by the structural changes in the hydrophobic core. This was the first direct structural prove for the previously observed perturbation of the membrane permeability induced by Aβ(25–35).

Applying the same technique, i.e., neutron diffraction in conjunction with selective deuteration, we demonstrated that cholesterol alters at the molecular level the capability of Aβ(25–35) to penetrate into the lipid bilayers [164]; in particular, a molar content of 20% of cholesterol hinders completely the intercalation of monomeric Aβ(25–35). Even at the low cholesterol content of only 5 mol% the penetration of Aβ(25–35) is strongly suppressed. These results link a structural property of a membrane to a physiological and functional behaviour, and point to a therapeutical approach to prevent the AD by modulation of membrane properties.

Finally, the influence of Aβ(1–42), the most abundant Aβ form in senile plaques, on unilamellar vesicles of phospholipids was investigated by small-angle neutron scattering [165]. We used the recently proposed separated form factor method to fit the data and to obtain information about the vesicle diameter and structure of the lipid bilayer and its change upon peptide administration. The lipid membrane parameters were fitted using different models of the bilayer profile. As a result, an increase of the vesicle radii, indicating vesicle fusion was obtained. This effect was particularly enhanced at pH 7.0 and at a high peptide/lipid ratio. At the same time, a thinning of the lipid bilayer occurred. The fusogenic activity of the peptide may have very important consequences and contribute to cytotoxicity by destabilising the cell and mitochondrial membranes. The perturbation of the bilayer structure suggests a strong interaction and/or insertion of the longer peptide into the membrane.

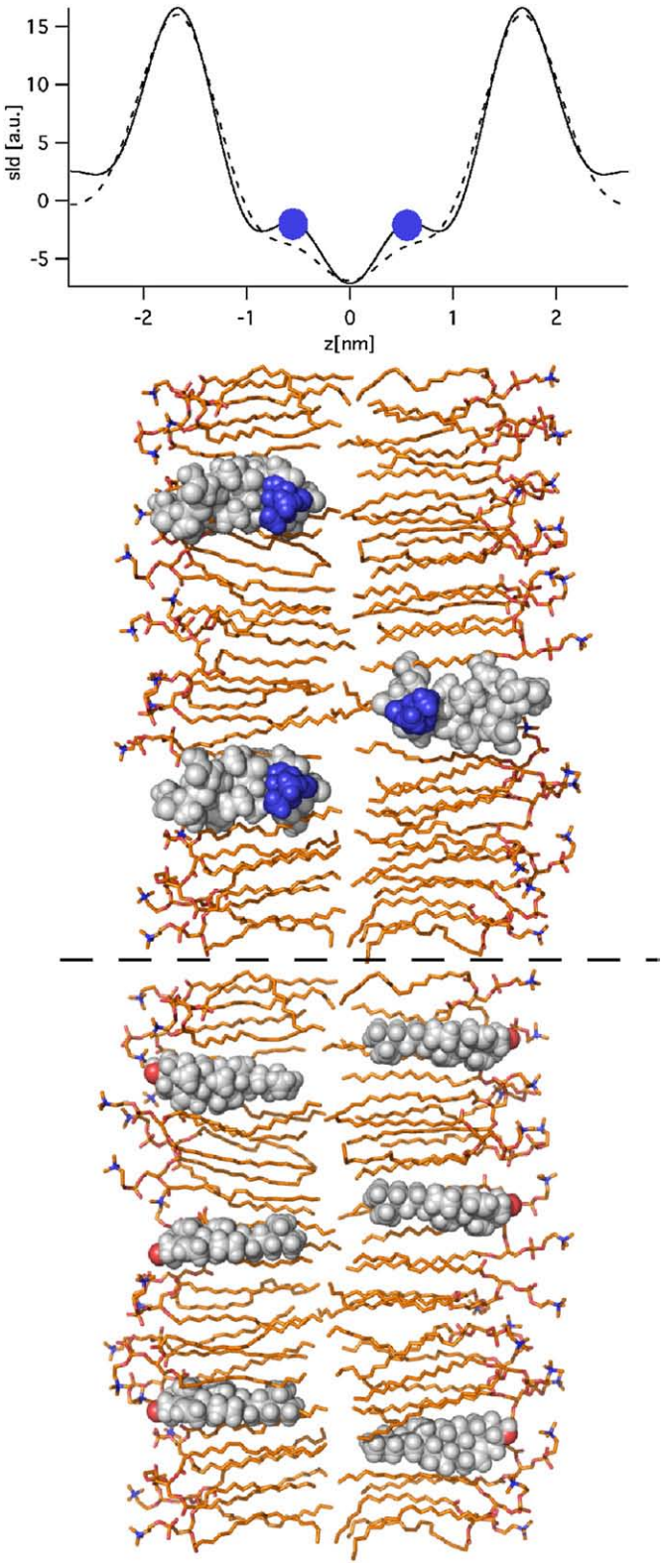

Fig. 5. Schematic drawing of a POPC/POPS (92:8 mol/mol) lipid bilayer containing cholesterol, in which intercalation of Aβ(25–35) is hindered (bottom). In the absence of cholesterol Aβ (25–35) can reach the hydrophobic core of the membrane (top). The atoms coloured in blue correspond to the deuterated amino acid (Leu34). The scattering length density profiles (sld) of the lipid bilayers with protonated (dashed profile) and deuterated (continuous line) peptide are drawn (upper top). The difference between the sld profiles is marked with a blue dot at the position of the Leu34 (from [164]).

Our results presented are in line with and do explain at the molecular level, at least in part, that Aβ is known to localise to mitochondrial membranes, block the transport of nuclear-encoded mitochondrial proteins to mitochondria, interact with mitochondrial proteins, disrupt the electron transport chain, increase reactive oxygen species (ROS) production, cause mitochondrial damage and prevent neurons from functioning normally [157]. Accumulation of monomeric Aβ within rat brain und muscle mitochondria has been demonstrated, concomitant with an increase in membrane viscosity, decrease in ATP/O, respiratory chain complexes inhibition, potentialization of ROS generation and cytochrome *c* release [166]. In mice brain, mitochondrial dysfunction related to Aβ was associated with higher levels of ROS and reduction in COX IV activity as well as ATP-levels [167]. From all the results accumulated, it is quite obvious that the bioenergetics of target cells and mitochondria are heavily perturbed by action of Aβ and by ageing.

Acknowledgements

This work was supported by the Deutsche Forschungsgemeinschaft grant SFB 472 to N.A.D. and H.S and EC FP6 contract number LSHM-CT-2004-512020, MiMage, to N.A.D.

References

[1] C.H. Fiske, Y. Subbarow, Phosphorus compounds of muscle and liver, Science 70 (1929) 381–382.
[2] K. Lohmann, Über die Pyrophosphatfraktion im Muskel, Naturwissenschaften 17 (1929) 624–625.
[3] P. Mitchell, Coupling of phosphorylation to electron and hydrogen transfer by a chemi-osmotic type of mechanism, Nature 191 (1961) 144–148.
[4] P.D. Boyer, R.L. Cross, W. Momsen, A new concept for energy coupling in oxidative phosphorylation based on a molecular explanation of the oxygen exchange reactions, Proc. Natl. Acad. Sci. U. S. A. 70 (1973) 2837–2839.
[5] P.D. Boyer, B.O. Stokes, R.G. Wolcott, C. Degani, Coupling of "high-energy" phosphate bonds to energy transductions, Fed. Proc. 34 (1975) 1711–1717.
[6] P.D. Boyer, A perspective of the binding change mechanism for ATP synthesis, FASEB J. 3 (1989) 2164–2178.
[7] S. Kerscher, S. Dröse, V. Zickermann, U. Brandt, The three families of respiratory NADH dehydrogenases, Results Probl. Cell Differ. 45 (2008) 185–222.
[8] U. Brandt, Energy converting NADH:quinone oxidoreductase (complex I), Annu. Rev. Biochem. 75 (2006) 69–92.
[9] D. Schneider, T. Pohl, J. Walter, K. Dörner, M. Kohlstädt, A. Berger, V. Spehr, T. Friedrich, Assembly of the *Escherichia coli* NADH:ubiquinone oxidoreductase (complex I), Biochim. Biophys. Acta 1777 (2008) 735–739.
[10] R.O. Vogel, J.A.M. Smeltink, L.G.J. Nijtmans, Human mitochondrial complex I assembly: a dynamic and versatile process, Biochim. Biophys. Acta, Bioenerg. 1767 (2007) 1215–1227.
[11] C. Remacle, M.R. Barbieri, P. Cardol, P.P. Hamel, Eukaryotic complex I: functional diversity and experimental systems to unravel the assembly process, Mol. Genet. Genomics 280 (2008) 93–110.
[12] M. Radermacher, T. Ruiz, T. Clason, S. Benjamin, U. Brandt, V. Zickermann, The three-dimensional structure of complex I from *Yarrowia lipolytica*: a highly dynamic enzyme, J. Struct. Biol. 154 (2006) 269–279.
[13] D.J. Morgan, L.A. Sazanov, Three-dimensional structure of respiratory complex I from *Escherichia coli* in ice in the presence of nucleotides, Biochim. Biophys. Acta 1777 (2008) 711–718.
[14] T. Pohl, D. Schneider, R. Hielscher, S. Stolpe, K. Dörner, M. Kohlstädt, B. Böttcher, P. Hellwig, T. Friedrich, Nucleotide-induced conformational changes in the *Escherichia coli* NADH:ubiquinone oxidoreductase (complex I), Biochem. Soc. Trans. 36 (2008) 971–975.
[15] N. Grigorieff, Three-dimensional structure of bovine NADH:ubiquinone oxidoreductase (complex I) at 22 Å in ice, J. Mol. Biol. 277 (1998) 1033–1046.
[16] L.A. Sazanov, P. Hinchliffe, Structure of the hydrophilic domain of respiratory complex I from *Thermus thermophilus*, Science 311 (2006) 1430–1436.
[17] T. Clason, V. Zickermann, T. Ruiz, U. Brandt, M. Radermacher, Direct localization of the 51 and 24 kDa subunits of mitochondrial complex I by three-dimensional difference imaging, J. Struct. Biol. 159 (2007) 433–442.
[18] C.R. Lancaster, A. Kröger, M. Auer, H. Michel, Structure of fumarate reductase from *Wolinella succinogenes* at 2.2 Å resolution, Nature 402 (1999) 377–385.
[19] F. Sun, X. Huo, Y. Zhai, A. Wang, J. Xu, D. Su, M. Bartlam, Z. Rao, Crystal structure of mitochondrial respiratory membrane protein complex II, Cell 121 (2005) 1043–1057.
[20] S. Iwata, J.W. Lee, K. Okada, J.K. Lee, M. Iwata, B. Rasmussen, T.A. Link, S. Ramaswamy, B.K. Jap, Complete structure of the 11-subunit bovine mitochondrial cytochrome bc_1 complex, Science 281 (1998) 64–71.
[21] D. Xia, C.A. Yu, H. Kim, J.Z. Xia, A.M. Kachurin, L. Zhang, L. Yu, J. Deisenhofer, Crystal structure of the cytochrome bc_1 complex from bovine heart mitochondria, Science 277 (1997) 60–66.
[22] Z. Zhang, L. Huang, V.M. Shulmeister, Y.I. Chi, K.K. Kim, L.W. Hung, A.R. Crofts, E.A. Berry, S.H. Kim, Electron transfer by domain movement in cytochrome bc_1, Nature 392 (1998) 677–684.
[23] C. Hunte, J. Koepke, C. Lange, T. Rossmanith, H. Michel, Structure at 2.3 Å resolution of the cytochrome bc_1 complex from the yeast *Saccharomyces cerevisiae* co-crystallized with an antibody Fv fragment, Structure 8 (2000) 669–684.
[24] S. Iwata, C. Ostermeier, B. Ludwig, H. Michel, Structure at 2.8 Å resolution of cytochrome *c* oxidase from *Paracoccus denitrificans*, Nature 376 (1995) 660–669.
[25] M. Svensson-Ek, J. Abramson, G. Larsson, S. Törnroth, P. Brzezinski, S. Iwata, The X-ray crystal structures of wild-type and EQ(I-286) mutant cytochrome *c* oxidases from *Rhodobacter sphaeroides*, J. Mol. Biol. 321 (2002) 329–339.
[26] T. Tsukihara, H. Aoyama, E. Yamashita, T. Tomizaki, H. Yamaguchi, K. Shinzawa-Itoh, R. Nakashima, R. Yaono, S. Yoshikawa, The whole structure of the 13-subunit oxidized cytochrome *c* oxidase at 2.8 Å, Science 272 (1996) 1136–1144.
[27] J.P. Abrahams, A.G. Leslie, R. Lutter, J.E. Walker, Structure at 2.8 Å resolution of F_1-ATPase from bovine heart mitochondria, Nature 370 (1994) 621–628.
[28] M.A. Bianchet, J. Hullihen, P.L. Pedersen, L.M. Amzel, The 2.8-Å structure of rat liver F_1-ATPase: configuration of a critical intermediate in ATP synthesis/hydrolysis, Proc. Natl. Acad. Sci. U. S. A. 95 (1998) 11065–11070.
[29] D. Stock, A.G. Leslie, J.E. Walker, Molecular architecture of the rotary motor in ATP synthase, Science 286 (1999) 1700–1705.
[30] V.K. Dickson, J.A. Silvester, I.M. Fearnley, A.G. Leslie, J.E. Walker, On the structure of the stator of the mitochondrial ATP synthase, EMBO J. 25 (2006) 2911–2918.
[31] J.L. Rubinstein, J.E. Walker, R. Henderson, Structure of the mitochondrial ATP synthase by electron cryomicroscopy, EMBO J. 22 (2003) 6182–6192.
[32] L.A. Baker, J.L. Rubinstein, Angle determination for side views in single particle electron microscopy, J. Struct. Biol. 162 (2008) 260–270.
[33] N.A. Dencher, H.J. Sass, G. Büldt, Water and bacteriorhodopsin: structure, dynamics, and function, Biochim. Biophys. Acta 1460 (2000) 192–203.
[34] E. Racker, W. Stoeckenius, Reconstitution of purple membrane vesicles catalyzing light-driven proton uptake and adenosine triphosphate formation, J. Biol. Chem. 249 (1974) 662–663.
[35] N. Dencher, M. Wilms, Flash photometric experiments on the photochemical cycle of bacteriorhodopsin, Biophys Struct Mech 1 (1975) 259–271.
[36] S. Grzesiek, N.A. Dencher, Monomeric and aggregated bacteriorhodopsin: single-turnover proton transport stoichiometry and photochemistry, Proc. Natl. Acad. Sci. U. S. A. 85 (1988) 9509–9513.
[37] J. Heberle, N.A. Dencher, Surface-bound optical probes monitor proton translocation and surface potential changes during the bacteriorhodopsin photocycle, Proc. Natl. Acad. Sci. U. S. A. 89 (1992) 5996–6000.
[38] J. Heberle, J. Riesle, G. Thiedemann, D. Oesterhelt, N.A. Dencher, Proton migration along the membrane surface and retarded surface to bulk transfer, Nature 370 (1994) 379–382.
[39] E. Nachliel, M. Gutman, S. Kiryati, N.A. Dencher, Protonation dynamics of the extracellular and cytoplasmic surface of bacteriorhodopsin in the purple membrane, Proc. Natl. Acad. Sci. U. S. A. 93 (1996) 10747–10752.
[40] J. Riesle, D. Oesterhelt, N.A. Dencher, J. Heberle, D38 is an essential part of the proton translocation pathway in bacteriorhodopsin, Biochemistry 35 (1996) 6635–6643.
[41] S. Checover, E. Nachliel, N.A. Dencher, M. Gutman, Mechanism of proton entry into the cytoplasmic section of the proton-conducting channel of bacteriorhodopsin, Biochemistry 36 (1997) 13919–13928.
[42] B. Schätzler, N.A. Dencher, J. Tittor, D. Oesterhelt, S. Yaniv-Checover, E. Nachliel, M. Gutman, Subsecond proton-hole propagation in bacteriorhodopsin, Biophys. J. 84 (2003) 671–686.
[43] J. Fitter, R.E. Lechner, N.A. Dencher, Interactions of hydration water and biological membranes studied by neutron scattering, J. Phys. Chem. B 103 (1999) 8036–8050.
[44] G. Papadopoulos, N.A. Dencher, G. Zaccai, G. Büldt, Water molecules and exchangeable hydrogen ions at the active centre of bacteriorhodopsin localized by neutron diffraction. Elements of the proton pathway? J. Mol. Biol. 214 (1990) 15–19.
[45] M. Weik, G. Zaccai, N.A. Dencher, D. Oesterhelt, T. Hauß, Structure and hydration of the M-state of the bacteriorhodopsin mutant D96N studied by neutron diffraction, J. Mol. Biol. 275 (1998) 625–634.
[46] T. Hauß, G. Papadopoulos, S.A.W. Verclas, G. Büldt, N.A. Dencher, Neutron diffraction on purple membranes — essential water molecules in the light-driven proton pump bacteriorhodopsin, Physica, B 234 (1997) 217–219.
[47] S. Grzesiek, N.A. Dencher, Dependency of ΔpH-relaxation across vesicular membranes on the buffering power of bulk solutions and lipids, Biophys. J. 50 (1986) 265–276.
[48] M.A. van der Horst, I.H. van Stokkum, N.A. Dencher, K.J. Hellingwerf, Controlled reduction of the humidity induces a shortcut recovery reaction in the photocycle of photoactive yellow protein, Biochemistry 44 (2005) 9160–9167.
[49] M. Gottschalk, N.A. Dencher, B. Halle, Microsecond exchange of internal water molecules in bacteriorhodopsin, J. Mol. Biol. 311 (2001) 605–621.
[50] T.H. Haines, N.A. Dencher, Cardiolipin: a proton trap for oxidative phosphorylation, FEBS Lett. 528 (2002) 35–39.
[51] A. Corcelli, S. Lobasso, M.S. Saponetti, A. Leopold, N.A. Dencher, Glycocardiolipin modulates the surface interaction of the proton pumped by bacteriorhodopsin in purple membrane preparations, Biochim. Biophys. Acta 1768 (2007) 2157–2163.
[52] J. Fitter, O.P. Ernst, T. Hauß, R.E. Lechner, K.P. Hofmann, N.A. Dencher, Molecular motions and hydration of purple membranes and disk membranes studied by neutron scattering, Eur. Biophys. J. 27 (1998) 638–645.

[53] J. Fitter, S.A. Verclas, R.E. Lechner, H. Seelert, N.A. Dencher, Function and picosecond dynamics of bacteriorhodopsin in purple membrane at different lipidation and hydration, FEBS Lett. 433 (1998) 321–325.

[54] R.E. Lechner, J. Fitter, N.A. Dencher, T. Hauß, Dehydration of biological membranes by cooling: an investigation on the purple membrane, J. Mol. Biol. 277 (1998) 593–603.

[55] J. Fitter, S.A.W. Verclas, R.E. Lechner, G. Büldt, O.P. Ernst, K.P. Hofmann, N.A. Dencher, Bacteriorhodopsin and rhodopsin studied by incoherent neutron scattering: dynamical properties of ground states and light activated intermediates, Physica, B 266 (1999) 35–40.

[56] A. Buchsteiner, R.E. Lechner, T. Hauß, N.A. Dencher, Relationship between structure, dynamics and function of hydrated purple membrane investigated by neutron scattering and dielectric spectroscopy, J. Mol. Biol. 371 (2007) 914–923.

[57] J. Pieper, A. Buchsteiner, N.A. Dencher, R.E. Lechner, T. Hauß, Transient protein softening during the working cycle of a molecular machine, Phys. Rev. Lett. 100 (2008) 228103.

[58] J. Pieper, A. Buchsteiner, N.A. Dencher, R.E. Lechner and T. Hauß, Light-induced modulation of protein dynamics during the photocycle of bacteriorhodopsin, Photochem. Photobiol. 85 (2009) 590–597.

[59] W. Doster, M. Settles, Protein–water displacement distributions, Biochim. Biophys. Acta 1749 (2005) 173–186.

[60] J. Pieper, T. Hauß, A. Buchsteiner, K. Baczyński, K. Adamiak, R.E. Lechner, G. Renger, Temperature- and hydration-dependent protein dynamics in photosystem II of green plants studied by quasielastic neutron scattering, Biochemistry 46 (2007) 11398–11409.

[61] W. Doster, S. Cusack, W. Petry, Dynamical transition of myoglobin revealed by inelastic neutron scattering, Nature 337 (1989) 754–756.

[62] J. Fitter, R.E. Lechner, G. Büldt, N.A. Dencher, Internal molecular motions of bacteriorhodopsin: hydration-induced flexibility studied by quasielastic incoherent neutron scattering using oriented purple membranes, Proc. Natl. Acad. Sci. U. S. A. 93 (1996) 7600–7605.

[63] J. Fitter, R.E. Lechner, N.A. Dencher, Picosecond molecular motions in bacteriorhodopsin from neutron scattering, Biophys. J. 73 (1997) 2126–2137.

[64] M. Ferrand, A.J. Dianoux, W. Petry, G. Zaccai, Thermal motions and function of bacteriorhodopsin in purple membranes: effects of temperature and hydration studied by neutron scattering, Proc. Natl. Acad. Sci. U. S. A. 90 (1993) 9668–9672.

[65] N.A. Dencher, D. Dresselhaus, G. Zaccai, G. Büldt, Structural changes in bacteriorhodopsin during proton translocation revealed by neutron diffraction, Proc. Natl. Acad. Sci. U. S. A. 86 (1989) 7876–7879.

[66] H.J. Sass, I.W. Schachowa, G. Rapp, M.H. Koch, D. Oesterhelt, N.A. Dencher, G. Büldt, The tertiary structural changes in bacteriorhodopsin occur between M states: X-ray diffraction and Fourier transform infrared spectroscopy, EMBO J. 16 (1997) 1484–1491.

[67] T.H. Haines, Do sterols reduce proton and sodium leaks through lipid bilayers? Prog. Lipid Res. 40 (2001) 299–324.

[68] S. Clejan, T.A. Krulwich, K.R. Mondrus, D. Seto-Young, Membrane lipid composition of obligately and facultatively alkalophilic strains of *Bacillus* spp, J. Bacteriol. 168 (1986) 334–340.

[69] G. Lenaz, A critical appraisal of the mitochondrial coenzyme Q pool, FEBS Lett. 509 (2001) 151–155.

[70] P.J. Quinn, in: V.E. Kagan, P.J. Quinn (Eds.), Coenzyme Q: Molecular Mechanisms in Health and Disease, CRC Press, New York, 2000, pp. 29–42.

[71] T. Hauß, S. Dante, N.A. Dencher, T.H. Haines, Squalane is in the midplane of the lipid bilayer: implications for its function as a proton permeability barrier, Biochim. Biophys. Acta 1556 (2002) 149–154.

[72] T. Hauß, S. Dante, T.H. Haines, N.A. Dencher, Localization of coenzyme Q_{10} in the center of a deuterated lipid membrane by neutron diffraction, Biochim. Biophys. Acta 1710 (2005) 57–62.

[73] E.A. Schon, N.A. Dencher, Heavy breathing: energy conversion by mitochondrial respiratory supercomplexes, Cell Metab. 9 (2009) 1–3.

[74] C.R. Hackenbrock, B. Chazotte, S.S. Gupte, The random collision model and a critical assessment of diffusion and collision in mitochondrial electron transport, J. Bioenerg. Biomembr. 18 (1986) 331–368.

[75] S. Gupte, E.S. Wu, L. Hoechli, M. Hoechli, K. Jacobson, A.E. Sowers, C.R. Hackenbrock, Relationship between lateral diffusion, collision frequency, and electron transfer of mitochondrial inner membrane oxidation–reduction components, Proc. Natl. Acad. Sci. U. S. A. 81 (1984) 2606–2610.

[76] A. Lass, R.S. Sohal, Comparisons of coenzyme Q bound to mitochondrial membrane proteins among different mammalian species, Free Radic. Biol. Med. 27 (1999) 220–226.

[77] A. Poetsch, H. Seelert, J. Meyer zu Tittingdorf, N.A. Dencher, Detergent effect on anion exchange perfusion chromatography and gel filtration of intact chloroplast H^+-ATP synthase, Biochem. Biophys. Res. Commun. 265 (1999) 520–524.

[78] H. Seelert, A. Poetsch, M. Rohlfs, N.A. Dencher, Dye–ligand chromatographic purification of intact multisubunit membrane protein complexes: application to the chloroplast H^+-F_OF_1-ATP synthase, Biochem. J. 346 (2000) 41–44.

[79] J.M. Meyer zu Tittingdorf, S. Rexroth, E. Schäfer, R. Schlichting, C. Giersch, N.A. Dencher, H. Seelert, The stoichiometry of the chloroplast ATP synthase oligomer III in *Chlamydomonas reinhardtii* is not affected by the metabolic state, Biochim. Biophys. Acta 1659 (2004) 92–99.

[80] T. Suhai, N.A. Dencher, A. Poetsch, H. Seelert, Remarkable stability of the proton translocating F_1F_O-ATP synthase from the thermophilic cyanobacterium *Thermosynechococcus elongatus* BP-1, Biochim. Biophys. Acta 1778 (2008) 1131–1140.

[81] P. Fromme, E.J. Boekema, P. Gräber, Isolation and characterization of a supramolecular complex of subunit III of the ATP synthase from chloroplasts, Zeitschrift für Naturforschung Teil. C 42c (1987) 1239–1245.

[82] H. Lill, W. Junge, Identification of a proteolipid oligomer as a constituent part of CF_O, the proton channel of the chloroplast ATP synthase, FEBS Lett. 244 (1989) 15–20.

[83] H. Seelert, A. Poetsch, N.A. Dencher, A. Engel, H. Stahlberg, D.J. Müller, Structural biology. Proton-powered turbine of a plant motor, Nature 405 (2000) 418–419.

[84] A. Poetsch, S. Rexroth, J. Heberle, T.A. Link, N.A. Dencher, H. Seelert, Characterisation of subunit III and its oligomer from spinach chloroplast ATP synthase, Biochim. Biophys. Acta 1618 (2003) 59–66.

[85] D. Pogoryelov, J. Yu, T. Meier, J. Vonck, P. Dimroth, D.J. Müller, The c_{15} ring of the *Spirulina platensis* F-ATP synthase: F_1/F_O symmetry mismatch is not obligatory, EMBO Rep. 6 (2005) 1040–1044.

[86] B. Varco-Merth, R. Fromme, M. Wang, P. Fromme, Crystallization of the c_{14}-rotor of the chloroplast ATP synthase reveals that it contains pigments, Biochim. Biophys. Acta 1777 (2008) 605–612.

[87] D. Pogoryelov, C. Reichen, A.L. Klyszejko, R. Brunisholz, D.J. Müller, P. Dimroth, T. Meier, The oligomeric state of c rings from cyanobacterial F-ATP synthases varies from 13 to 15, J. Bacteriol. 189 (2007) 5895–5902.

[88] T. Meier, U. Matthey, C. von Ballmoos, J. Vonck, T. Krug von Nidda, W. Kühlbrandt, P. Dimroth, Evidence for structural integrity in the undecameric c-rings isolated from sodium ATP synthases, J. Mol. Biol. 325 (2003) 389–397.

[89] T. Meier, P. Polzer, K. Diederichs, W. Welte, P. Dimroth, Structure of the rotor ring of F-Type Na^+-ATPase from *Ilyobacter tartaricus*, Science 308 (2005) 659–662.

[90] H. Seelert, N.A. Dencher, D.J. Müller, Fourteen protomers compose the oligomer III of the proton-rotor in spinach chloroplast ATP synthase, J. Mol. Biol. 333 (2003) 337–344.

[91] H. Seelert, F. Krause, Preparative isolation of protein complexes and other bioparticles by elution from polyacrylamide gels, Electrophoresis 29 (2008) 2617–2636.

[92] F. Krause, H. Seelert, in: J.E. Coligan, B.M. Dunn, D.W. Speicher, P.T. Wingfield (Eds.), Current Protocols in Protein Science, John Wiley and Sons, Inc., 2008, pp. UNIT 14.11: 1–36; republished as UNIT 19.18.

[93] F. Krause, Detection and analysis of protein–protein interactions in organellar and prokaryotic proteomes by native gel electrophoresis: (membrane) protein complexes and supercomplexes, Electrophoresis 27 (2006) 2759–2781.

[94] D. Neff, N.A. Dencher, Purification of multisubunit membrane protein complexes: isolation of chloroplast F_OF_1-ATP synthase, CF_O and CF_1 by blue native electrophoresis, Biochem. Biophys. Res. Commun. 259 (1999) 569–575.

[95] H. Schägger, G. von Jagow, Blue native electrophoresis for isolation of membrane protein complexes in enzymatically active form, Anal. Biochem. 199 (1991) 223–231.

[96] A. Poetsch, D. Neff, H. Seelert, H. Schägger, N.A. Dencher, Dye removal, catalytic activity and 2D crystallization of chloroplast H^+-ATP synthase purified by blue native electrophoresis, Biochim. Biophys. Acta 1466 (2000) 339–349.

[97] W. Junge, H. Lill, S. Engelbrecht, ATP synthase: an electrochemical transducer with rotatory mechanics, Trends Biochem. Sci. 22 (1997) 420–423.

[98] J. Weber, ATP synthase—the structure of the stator stalk, Trends Biochem. Sci. 32 (2007) 53–56.

[99] A. Poetsch, R.J. Berzborn, J. Heberle, T.A. Link, N.A. Dencher, H. Seelert, Biophysics and bioinformatics reveal structural differences of the two peripheral stalk subunits in chloroplast ATP synthase, J. Biochem. 141 (2007) 411–420.

[100] M. Gertz, H. Seelert, N.A. Dencher, A. Poetsch, Interactions of rotor subunits in the chloroplast ATP synthase modulated by nucleotides and by Mg^{2+}, Biochim. Biophys. Acta 1774 (2007) 566–574.

[101] X.B. Shi, J.M. Wei, Y.K. Shen, Effects of sequential deletions of residues from the N- or C-terminus on the functions of ε subunit of the chloroplast ATP synthase, Biochemistry 40 (2001) 10825–10831.

[102] S. Cadenas, M.D. Brand, Effects of magnesium and nucleotides on the proton conductance of rat skeletal-muscle mitochondria, Biochem. J. 348 (Pt 1) (2000) 209–213.

[103] X.H. Ma, Y.L. Shi, Effects of ADP, DTT, and Mg^{2+} on the ion-conductive property of chloroplast H^+-ATPase CF_O-CF_1 reconstituted into bilayer membrane, Biochem. Biophys. Res. Commun. 232 (1997) 461–463.

[104] D. Neff, S. Tripathi, K. Middendorf, H. Stahlberg, H.J. Butt, E. Bamberg, N.A. Dencher, Chloroplast F_OF_1 ATP synthase imaged by atomic force microscopy, J. Struct. Biol. 119 (1997) 139–148.

[105] W. Jiang, J. Hermolin, R.H. Fillingame, The preferred stoichiometry of c subunits in the rotary motor sector of *Escherichia coli* ATP synthase is 10, Proc. Natl. Acad. Sci. U. S. A. 98 (2001) 4966–4971.

[106] P. Turina, D. Samoray, P. Gräber, H^+/ATP ratio of proton transport-coupled ATP synthesis and hydrolysis catalysed by CF_0F_1-liposomes, EMBO J. 22 (2003) 418–426.

[107] W. Junge, O. Pänke, D.A. Cherepanov, K. Gumbiowski, M. Müller, S. Engelbrecht, Inter-subunit rotation and elastic power transmission in F_0F_1-ATPase, FEBS Lett. 504 (2001) 152–160.

[108] H. Seelert, S. Rexroth, N.A. Dencher, D.J. Müller, W. Kühlbrandt, J. Vonck, Characterization of the α-helices in the proton turbine of chloroplast F_OF_1 ATP synthase, Biol. Chem. Hoppe-Seyler, Suppl. 382 (2001) S147.

[109] A. Laisk, H. Eichelmann, V. Oja, E. Talts, R. Scheibe, Rates and roles of cyclic and alternative electron flow in potato leaves, Plant Cell Physiol. 48 (2007) 1575–1588.

[110] S. Steigmiller, P. Turina, P. Gräber, The thermodynamic H^+/ATP ratios of the H^+-ATPsynthases from chloroplasts and *Escherichia coli*, Proc. Natl. Acad. Sci. U. S. A. 105 (2008) 3745–3750.

[111] J. Vonck, T.K. von Nidda, T. Meier, U. Matthey, D.J. Mills, W. Kühlbrandt, P. Dimroth, Molecular architecture of the undecameric rotor of a bacterial Na^+-ATP synthase, J. Mol. Biol. 321 (2002) 307–316.

[112] T. Meier, S.A. Ferguson, G.M. Cook, P. Dimroth, J. Vonck, Structural investigations of the membrane-embedded rotor ring of the F-ATPase from *Clostridium paradoxum*, J. Bacteriol. 188 (2006) 7759–7764.
[113] M. Fritz, A.L. Klyszejko, N. Morgner, J. Vonck, B. Brutschy, D.J. Müller, T. Meier, V. Müller, An intermediate step in the evolution of ATPases: a hybrid F_O-V_O rotor in a bacterial Na^+ F_1F_O ATP synthase, FEBS J. 275 (2008) 1999–2007.
[114] M. Toei, C. Gerle, M. Nakano, K. Tani, N. Gyobu, M. Tamakoshi, N. Sone, M. Yoshida, Y. Fujiyoshi, K. Mitsuoka, K. Yokoyama, Dodecamer rotor ring defines H^+/ATP ratio for ATP synthesis of prokaryotic V-ATPase from T*hermus thermophilus*, Proc. Natl. Acad. Sci. U. S. A. 104 (2007) 20256–20261.
[115] N. Mitome, T. Suzuki, S. Hayashi, M. Yoshida, Thermophilic ATP synthase has a decamer c-ring: indication of noninteger 10:3 H^+/ATP ratio and permissive elastic coupling, Proc. Natl. Acad. Sci. U. S. A. 101 (2004) 12159–12164.
[116] T. Meier, N. Morgner, D. Matthies, D. Pogoryelov, S. Keis, G.M. Cook, P. Dimroth, B. Brutschy, A tridecameric c ring of the adenosine triphosphate (ATP) synthase from the thermoalkaliphilic *Bacillus* sp. strain TA2.A1 facilitates ATP synthesis at low electrochemical proton potential, Mol. Microbiol. 65 (2007) 1181–1192.
[117] S. Fischer, P. Gräber, Comparison of ΔpH- and Δϕ-driven ATP synthesis catalyzed by the H^+-ATPases from *Escherichia coli* or chloroplasts reconstituted into liposomes, FEBS Lett. 457 (1999) 327–332.
[118] J.A. Cruz, C.A. Sacksteder, A. Kanazawa, D.M. Kramer, Contribution of electric field ($\Delta\psi$) to steady-state transthylakoid proton motive force (pmf) in vitro and in vivo. control of pmf parsing into $\Delta\psi$ and ΔpH by ionic strength, Biochemistry 40 (2001) 1226–1237.
[119] C. von Ballmoos, G.M. Cook, P. Dimroth, Unique rotary ATP synthase and its biological diversity, Annu. Rev. Biophys. 37 (2008) 43–64.
[120] G. Kaim, P. Dimroth, ATP synthesis by F-type ATP synthase is obligatorily dependent on the transmembrane voltage, EMBO J. 18 (1999) 4118–4127.
[121] S.J. Ferguson, ATP synthase: what dictates the size of a ring? Curr. Biol. 10 (2000) 804–808.
[122] D.J. Müller, N.A. Dencher, T. Meier, P. Dimroth, K. Suda, H. Stahlberg, A. Engel, H. Seelert, U. Matthey, ATP synthase: constrained stoichiometry of the transmembrane rotor, FEBS Lett. 504 (2001) 219–222.
[123] I. Arechaga, P.J. Butler, J.E. Walker, Self-assembly of ATP synthase subunit c rings, FEBS Lett. 515 (2002) 189–193.
[124] T. Suzuki, Y. Ozaki, N. Sone, B.A. Feniouk, M. Yoshida, The product of *uncI* gene in F_1F_O-ATP synthase operon plays a chaperone-like role to assist *c*-ring assembly, Proc. Natl. Acad. Sci. U. S. A. 104 (2007) 20776–20781.
[125] Y. Ozaki, T. Suzuki, Y. Kuruma, T. Ueda, M. Yoshida, UncI protein can mediate ring-assembly of c-subunits of F_OF_1-ATP synthase in vitro, Biochem. Biophys. Res. Commun. 367 (2008) 663–666.
[126] R.A. Schemidt, D.K. Hsu, G. Deckers-Hebestreit, K. Altendorf, W.S. Brusilow, The effects of an atpE ribosome-binding site mutation on the stoichiometry of the c subunit in the F_1F_0 ATPase of *Escherichia coli*, Arch. Biochem. Biophys. 323 (1995) 423–428.
[127] R.A. Schemidt, J. Qu, J.R. Williams, W.S. Brusilow, Effects of carbon source on expression of F_0 genes and on the stoichiometry of the c subunit in the F_1F_0 ATPase of *Escherichia coli*, J. Bacteriol. 180 (1998) 3205–3208.
[128] T. Meier, J. Yu, T. Raschle, F. Henzen, P. Dimroth, D.J. Müller, Structural evidence for a constant c_{11} ring stoichiometry in the sodium F-ATP synthase, FEBS J. 272 (2005) 5474–5483.
[129] T. Krebstakies, I. Aldag, K. Altendorf, J.C. Greie, G. Deckers-Hebestreit, The stoichiometry of subunit c of *Escherichia coli* ATP synthase is independent of its rate of synthesis, Biochemistry 47 (2008) 6907–6916.
[130] M. Vázquez-Acevedo, P. Cardol, A. Cano-Estrada, M. Lapaille, C. Remacle, D. González-Halphen, The mitochondrial ATP synthase of chlorophycean algae contains eight subunits of unknown origin involved in the formation of an atypical stator-stalk and in the dimerization of the complex, J. Bioenerg. Biomembr. 38 (2006) 271–282.
[131] R. van Lis, A. Atteia, G. Mendoza-Hernandez, D. Gonzalez-Halphen, Identification of novel mitochondrial protein components of *Chlamydomonas reinhardtii*. A proteomic approach, Plant Physiol. 132 (2003) 318–330.
[132] S. Rexroth, J.M.W. Meyer zu Tittingdorf, F. Krause, N.A. Dencher, H. Seelert, Thylakoid membrane at altered metabolic state: challenging the forgotten realms of the proteome, Electrophoresis 24 (2003) 2814–2823.
[133] H. Schägger, Respiratory chain supercomplexes of mitochondria and bacteria, Biochim. Biophys. Acta 1555 (2002) 154–159.
[134] I. Wittig, R. Carrozzo, F.M. Santorelli, H. Schägger, Supercomplexes and subcomplexes of mitochondrial oxidative phosphorylation, Biochim. Biophys. Acta 1757 (2006) 1066–1072.
[135] F. Krause, in: M.I.G. Siso (Ed.), Complex I and Alternative NADH Dehydrogenases, Transworld Research Network, Kerala, India, 2007, pp. 179–213.
[136] I. Grotjohann, P. Gräber, The H^+-ATPase from chloroplasts: effect of different reconstitution procedures on ATP synthesis activity and on phosphate dependence of ATP synthesis, Biochim. Biophys. Acta 1556 (2002) 208–216.
[137] S. Rexroth, J.M. Meyer zu Tittingdorf, H.J. Schwaßmann, F. Krause, H. Seelert, N.A. Dencher, Dimeric H^+-ATP synthase in the chloroplast of *Chlamydomonas reinhardtii*, Biochim. Biophys. Acta 1658 (2004) 202–211.
[138] H.J. Schwaßmann, S. Rexroth, H. Seelert, N.A. Dencher, Metabolism controls dimerization of the chloroplast F_OF_1 ATP synthase in *Chlamydomonas reinhardtii*, FEBS Lett. 581 (2007) 1391–1396.
[139] F. Krause, N.H. Reifschneider, S. Goto, N.A. Dencher, Active oligomeric ATP synthases in mammalian mitochondria, Biochem. Biophys. Res. Commun. 329 (2005) 583–590.
[140] N.H. Reifschneider, S. Goto, H. Nakamoto, R. Takahashi, M. Sugawa, N.A. Dencher, F. Krause, Defining the mitochondrial proteomes from five rat organs in a physiologically significant context using 2D blue-native/SDS-PAGE, J. Proteome Res. 5 (2006) 1117–1132.
[141] F. Krause, C.Q. Scheckhuber, A. Werner, S. Rexroth, N.H. Reifschneider, N.A. Dencher, H.D. Osiewacz, Supramolecular organization of cytochrome *c* oxidase- and alternative oxidase-dependent respiratory chains in the filamentous fungus *Podospora anserina*, J. Biol. Chem. 279 (2004) 26453–26461.
[142] M.F.P.M. Maas, F. Krause, N.A. Dencher and A. Sainsard-Chanet, Respiratory complexes III and IV are not essential for the assembly/stability of complex I in fungi, J. Mol. Biol. 387 (2009) 259–269.
[143] I. Marques, N.A. Dencher, A. Videira, F. Krause, Supramolecular organization of the respiratory chain in *Neurospora crassa* mitochondria, Eukaryotic Cell 6 (2007) 2391–2405.
[144] F. Krause, N.H. Reifschneider, D. Vocke, H. Seelert, S. Rexroth, N.A. Dencher, "Respirasome"-like supercomplexes in green leaf mitochondria of spinach, J. Biol. Chem. 279 (2004) 48369–48375.
[145] C. Hunzinger, W. Wozny, G.P. Schwall, S. Poznanović, W. Stegmann, H. Zengerling, R. Schoepf, K. Groebe, M.A. Cahill, H.D. Osiewacz, N. Jägemann, M. Bloch, N.A. Dencher, F. Krause, A. Schrattenholz, Comparative profiling of the mammalian mitochondrial proteome: multiple aconitase-2 isoforms including *N*-formyl-kynurenine modifications as part of a protein biomarker signature for reactive oxidative species, J. Proteome Res. 5 (2006) 625–633.
[146] E. Schäfer, H. Seelert, N.H. Reifschneider, F. Krause, N.A. Dencher, J. Vonck, Architecture of active mammalian respiratory chain supercomplexes, J. Biol. Chem. 281 (2006) 15370–15375.
[147] E. Schäfer, N.A. Dencher, J. Vonck, D.N. Parcej, Three-dimensional structure of the respiratory chain supercomplex $I_1III_2IV_1$ from bovine heart mitochondria, Biochemistry 46 (2007) 12579–12585.
[148] J. Vonck, E. Schäfer, Supramolecular organization of protein complexes in the mitochondrial inner membrane, Biochim. Biophys. Acta 1793 (2009) 117–124.
[149] M.L. Genova, A. Baracca, A. Biondi, G. Casalena, M. Faccioli, A.I. Falasca, G. Formiggini, G. Sgarbi, G. Solaini, G. Lenaz, Is supercomplex organization of the respiratory chain required for optimal electron transfer activity? Biochim. Biophys. Acta 1777 (2008) 740–746.
[150] N.A. Dencher, M. Frenzel, N.H. Reifschneider, M. Sugawa, F. Krause, Proteome alterations in rat mitochondria caused by aging, Ann. N.Y. Acad. Sci. 1100 (2007) 291–298.
[151] C. Wernicke, J. Hellmann, B. Zięba, K. Kuter, K. Ossowska, M. Frenzel, N.A. Dencher, G. Gille and H. Rommelspacher, 9-Methyl-β-carboline has restorative effects in an animal model of Parkinson's disease, European Journal of Neuroscience (submitted for publication).
[152] S. Viswanathan, M. Ünlü, J.S. Minden, Two-dimensional difference gel electrophoresis, Nat. Protoc. 1 (2006) 1351–1358.
[153] D. Dani, N.A. Dencher, Native-DIGE: a new look at the mitochondrial membrane proteome, Biotechnol. J. 3 (2008) 817–822.
[154] D. Dani, I. Shimokawa, T. Komatsu, Y. Higami, U. Warnken, E. Schokraie, M. Schnölzer, F. Krause, M. Sugawa, N.A. Dencher, Trade-off between calorie restriction and ageing in rat liver mitochondria, Mech. Aging Devel. (submitted for publication).
[155] K. Groebe, F. Krause, B. Kunstmann, H. Unterluggauer, N.H. Reifschneider, C.Q. Scheckhuber, C. Sastri, W. Stegmann, W. Wozny, G.P. Schwall, S. Poznanovic, N.A. Dencher, P. Jansen-Dürr, H.D. Osiewacz, A. Schrattenholz, Differential proteomic profiling of mitochondria from *Podospora anserina*, rat and human reveals distinct patterns of age-related oxidative changes, Exp. Gerontol. 42 (2007) 887–898.
[156] X. Wang, B. Su, G. Perry, M.A. Smith, X. Zhu, Insights into amyloid-β-induced mitochondrial dysfunction in Alzheimer disease, Free Radic. Biol. Med. 43 (2007) 1569–1573.
[157] P.H. Reddy, M.F. Beal, Amyloid β, mitochondrial dysfunction and synaptic damage: implications for cognitive decline in aging and Alzheimer's disease, Trends Mol. Med. 14 (2008) 45–53.
[158] J. Busciglio, A. Lorenzo, J. Yeh, B.A. Yankner, β-amyloid fibrils induce tau phosphorylation and loss of microtubule binding, Neuron 14 (1995) 879–888.
[159] A. Abbott, Neuroscience: the plaque plan, Nature 456 (2008) 161–164.
[160] C. Haass, D.J. Selkoe, Soluble protein oligomers in neurodegeneration: lessons from the Alzheimer's amyloid β-peptide, Nat. Rev., Mol. Cell Biol. 8 (2007) 101–112.
[161] S. Dante, T. Hauß, N.A. Dencher, β-amyloid 25 to 35 is intercalated in anionic and zwitterionic lipid membranes to different extents, Biophys. J. 83 (2002) 2610–2616.
[162] R.P. Mason, R.F. Jacob, M.F. Walter, P.E. Mason, N.A. Avdulov, S.V. Chochina, U. Igbavboa, W.G. Wood, Distribution and fluidizing action of soluble and aggregated amyloid β-peptide in rat synaptic plasma membranes, J. Biol. Chem. 274 (1999) 18801–18807.
[163] S. Dante, T. Hauß, N.A. Dencher, Insertion of externally administered amyloid beta peptide 25–35 and perturbation of lipid bilayers, Biochemistry 42 (2003) 13667–13672.
[164] S. Dante, T. Hauß, N.A. Dencher, Cholesterol inhibits the insertion of the Alzheimer's peptide Aβ(25–35) in lipid bilayers, Eur. Biophys. J. 35 (2006) 523–531.
[165] S. Dante, T. Hauß, A. Brandt, N.A. Dencher, Membrane fusogenic activity of the Alzheimer's peptide A beta(1–42) demonstrated by small-angle neutron scattering, J. Mol. Biol. 376 (2008) 393–404.
[166] A.M. Aleardi, G. Benard, O. Augereau, M. Malgat, J.C. Talbot, J.P. Mazat, T. Letellier, J. Dachary-Prigent, G.C. Solaini, R. Rossignol, Gradual alteration of mitochondrial structure and function by β-amyloids: importance of membrane viscosity changes, energy deprivation, reactive oxygen species production, and cytochrome *c* release, J. Bioenerg. Biomembr. 37 (2005) 207–225.

[167] S. Hauptmann, I. Scherping, S. Dröse, U. Brandt, K.L. Schulz, M. Jendrach, K. Leuner, A. Eckert, W.E. Müller, Mitochondrial dysfunction: an early event in Alzheimer pathology accumulates with age in AD transgenic mice, Neurobiol. Aging (2008), doi:10.1016/j.neurobiolaging.2007.12.005.
[168] L.S. Huang, D. Cobessi, E.Y. Tung, E.A. Berry, Binding of the respiratory chain inhibitor antimycin to the mitochondrial bc_1 complex: a new crystal structure reveals an altered intramolecular hydrogen-bonding pattern, J. Mol. Biol. 351 (2005) 573–597.
[169] C. Lange, C. Hunte, Crystal structure of the yeast cytochrome bc_1 complex with its bound substrate cytochrome *c*, Proc. Natl. Acad. Sci. U. S. A. 99 (2002) 2800–2805.
[170] M. Frenzel, F. Krause, H. Rommelspacher, M. Sugawa, N.A. Dencher, unpublished results.